The mineralogical and lithogeochemical footprint of the George Fisher Zn-Pb-Ag massive sulphide deposit in the Proterozoic Urquhart Shale Formation, Queensland, Australia

Philip Rieger [a,b,*], Joseph M. Magnall [a], Sarah A. Gleeson [a,b], Anja M. Schleicher [a], Marie Bonitz [a,c], Richard Lilly [d]

[a] GFZ German Research Centre for Geosciences, Germany
[b] Institute of Geological Sciences, Freie Universität Berlin, Germany
[c] Department of Earth Sciences, University of Potsdam, Germany
[d] Department of Earth Sciences, University of Adelaide, Australia

ARTICLE INFO

ABSTRACT

The Proterozoic Carpentaria Province (McArthur basin and Mount Isa Inlier) in northern Australia comprises a number of world class clastic dominated (CD-type) Zn-Pb massive sulphide deposits, formally known as SEDEX deposits. In order to identify the geochemical footprint of any mineralizing system it is necessary to characterize compositional variability of the host-rock to mineralization. In the southern Carpentaria, establishing the baseline composition of the host rock is complicated by varying degrees of tectonic overprint, a lack of metamorphic indicator minerals, and the overall size of the ore forming systems. In this study, samples from drill-holes intersecting the main ore bodies at the world class George Fisher CD-type massive sulphide deposit have been compared to samples from a drill-hole intersecting barren, correlative lithologies of the Urquhart Shale Formation (ca. 1654 Ma). Bulk rock lithogeochemical (X-ray fluorescence, inductively coupled plasma mass spectrometry and LECO) and mineralogical (X-ray diffraction) analyses have been combined with petrographic observations to (1) establish the baseline composition of the Urquhart Shale Formation and (2) determine the geochemical and mineralogical footprint of the CD-type system at George Fisher. The absence of metamorphic indicator minerals, combined with the preservation of illite in un-mineralized Urquhart Shale, suggests that in this part of the Mount Isa area, the host rocks did not reach greenschist facies conditions ($>$300 °C). Chlorite in the un-mineralized Urquhart Shale is very fine grained ($\leq$ 10 µm) within interstitial pore spaces with other phyllosilicates (e.g., illite), and is interpreted to be diagenetic in origin. Relative to the un-mineralized Urquhart Shale, the first stage of sulphide mineralization (Zn-dominated, stratabound) at George Fisher is associated with decreased abundances of albite, chlorite, and calcite, and higher abundances of dolomite and phyllosilicates (muscovite and phlogopite). These mineralogical transformations are associated with strong minor and trace element depletion (Sr and Na) and enrichment (Tl and Mn). An element index based on this suite of elements (GF index $= 10\left(\frac{400Tl+Mn}{10Sr+Na}\right)$) is highly effective in differentiating between the background Urquhart Shale Formation and the alteration footprint at George Fisher and may provide an additional tool for geochemical exploration programmes in the Mount Isa area. This study affirms the benefit of combining lithogeochemical, mineralogical, and petrographic data in order to understand the host rock baseline composition and the alteration footprint of Carpentaria CD-type massive sulphide systems.

1. Introduction

The Proterozoic Urquhart Shale Formation is host to three world class base metal deposits (Mount Isa, Hilton, and George Fisher), which collectively have a pre-mining resource of >370 Mt. (10 wt% Zn, 5.6 wt % Pb, and 120 g/t Ag; Large et al., 2005). These clastic dominant (CD-
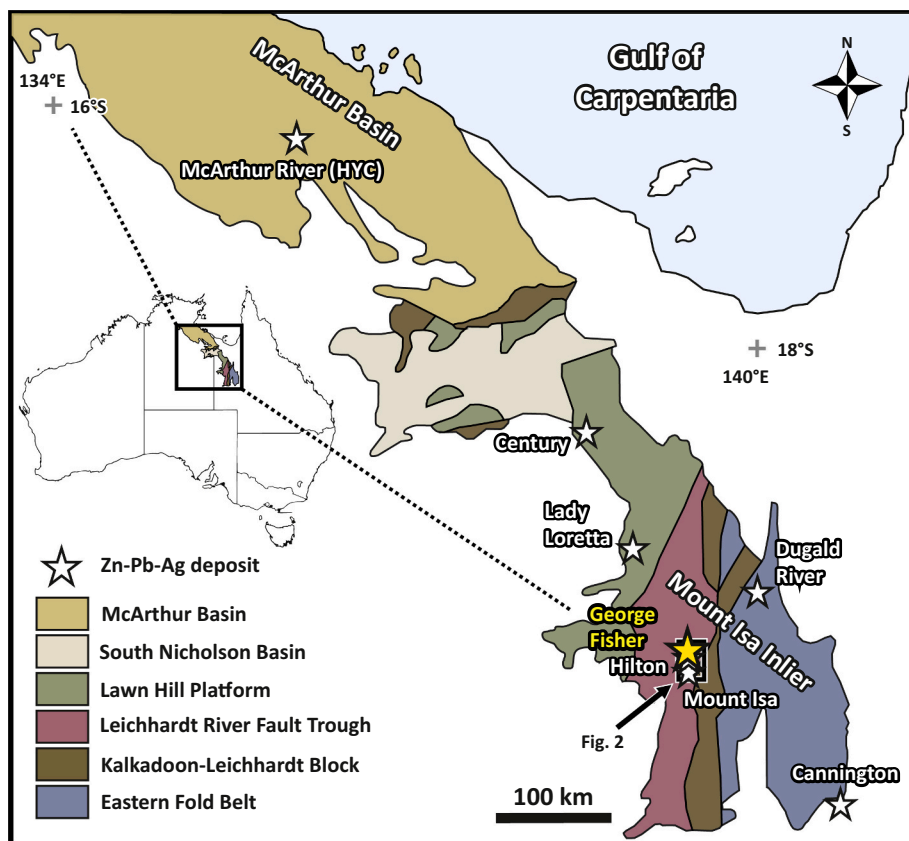

Fig. 1. Tectono-stratigraphic map of the Mount Isa Inlier and the McArthur basin with major Zn-Pb-Ag deposits marked by asterisks (Gibson et al., 2017; Jackson et al., 2000). The black rectangle indicates the Mount Isa region shown in Fig. 2.

type) deposits, formerly known as sedimentary exhalative (SEDEX) deposits (Leach et al., 2010), have accounted for a significant proportion of global Zn and Pb production and have been crucial in satisfying demand of these base metals for the global economy (Leach et al., 2005). Future demand will only be met through the discovery of new Zn-Pb deposits, although exploration models for Carpentaria CD-type massive sulphide deposits are currently limited by an incomplete understanding of the geochemical and mineralogical footprints to these systems.

The Mount Isa, Hilton, and George Fisher deposits are located in close proximity (ca. 20 km) in the Mount Isa Inlier, which is broadly time correlative with the McArthur basin (both basins comprise the Carpentaria Zn Province; Fig. 1). The tectonic and metamorphic gradient increases towards the south of the Carpentaria Province, which has resulted in considerable debate over the genetic model for the Carpentaria CD-type deposits; specifically, debate has mostly focused on the relative contribution of sedimentary exhalative (SEDEX; e.g., Lambert and Scott, 1973; Large et al., 1998), subseafloor diagenetic replacement processes (e.g., Chapman, 2004; Eldridge et al., 1993; Painter et al., 1999), or *syn*-deformational replacement (e.g., Cave et al., 2020; Perkins, 1998; Perkins and Bell, 1998).

The host rock to the Carpentaria deposits can be broadly characterized as a fine-grained, variably pyritic and dolomitic carbonaceous siltstone (Leach et al., 2010; Leach et al., 2005). Fine-grained siliciclastic rocks often appear to be relatively homogenous at the hand specimen scale, but they can preserve considerable compositional heterogeneity due to the variability of detrital, biogenic and authigenic components (e. g., Aplin and Macquaker, 2011; Vine and Tourtelot, 1970). Published lithogeochemical alteration models for the Carpentaria deposits have so far mostly been informed by the SEDEX model. For example, the enrichment of several elements (Co, Fe, Tl, Zn, Pb, and Mn) in dolomite and pyrite in correlative stratigraphy to the McArthur River and Lady

Table 1
Alteration indices and element ratios for the Carpentaria Province.

| Element abundance/ alteration index	Formula	Threshold	Reference
Relative abundance of Co and Ni	Co/Ni	>1	Lambert and Scott (1973)
Widely dispersed trace metal enrichment	Tl, Pb and Zn	Tl >4 ppm, Pb >100 ppm, Zn >1000 ppm	Large and McGoldrick (1998)
SEDEX metal index (SEDEX MI)	Zn + 100Pb + 100 Tl	>10,000	Large and McGoldrick (1998)
Manganese content of dolomite (MnO$_d$)	(MnO x 30.41)/CaO	>1.0 wt%	Large and McGoldrick (1998)
SEDEX alteration index (SEDEX AI)	$\dfrac{100(FeO + 10\,MnO)}{FeO + 10\,MnO + MgO}$	>60	Large and McGoldrick (1998)
SEDEX alteration index 3 (AI mark 3)	$\dfrac{100(FeO + 10\,MnO)}{FeO + 10\,MnO + MgO + Al_2O_3}$	>30	Large et al. (2000)
SEDEX alteration index 4 (AI mark 4)	$\dfrac{100(FeO + 10\,MnO)}{FeO + 10\,MnO + MgO + 0.1*SiO_2}$	–	Large et al. (2000)
Isa vector	$\dfrac{Tl(FeO_{dol} + 10\,MnO_d)}{Ge}$	–	Painter (2003)
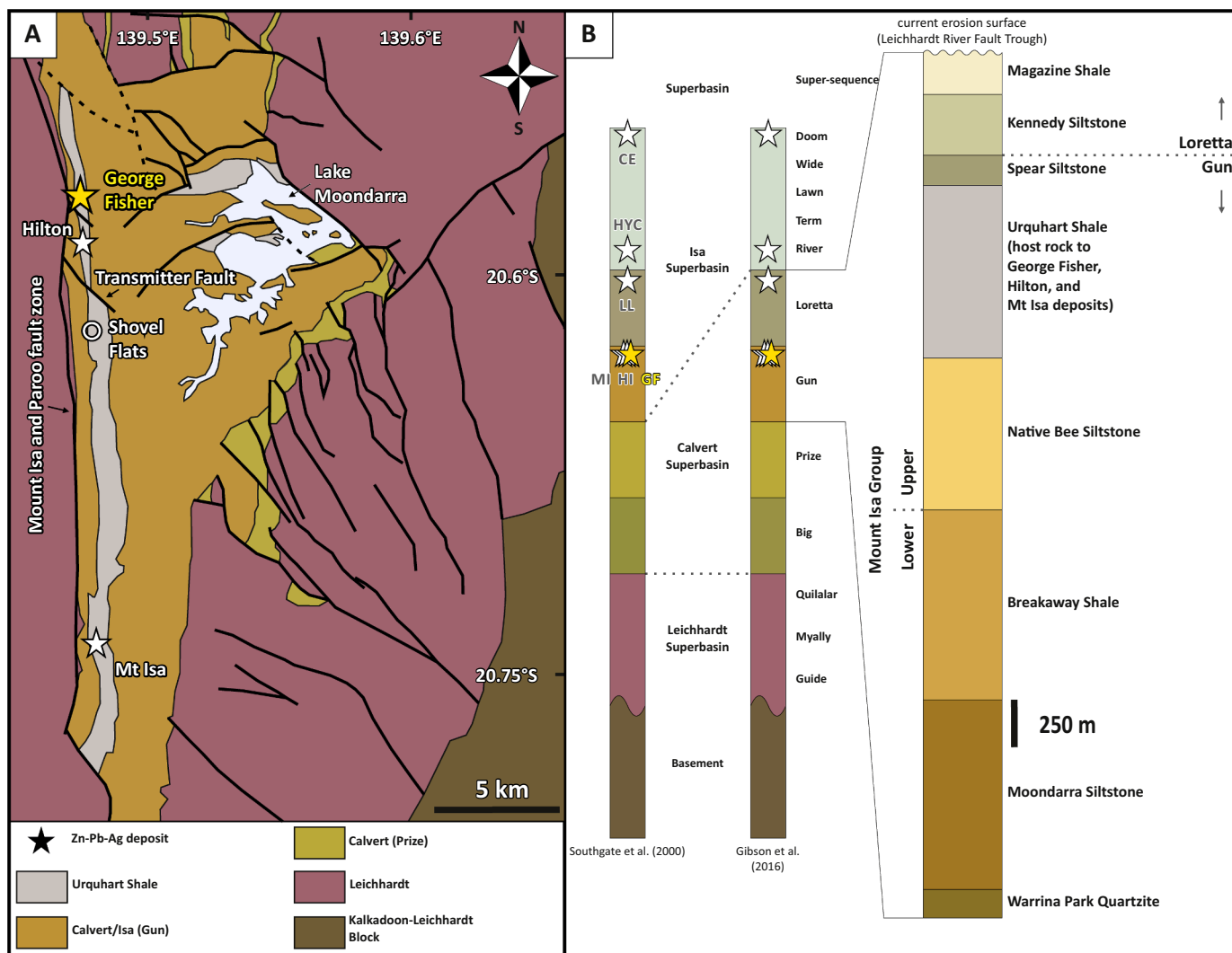
Fig. 2. A. Geological map of the Leichhardt River Fault Trough in the Mount Isa area (after Gibson et al., 2017, Gibson et al., 2016). The Mount Isa, Hilton, and George Fisher deposits and Shovel Flats drill-hole are marked by asterisks and a circle respectively. B. A stratigraphic chart for the Mount Isa Inlier showing superbasins and supersequences (after Gibson et al., 2016; Southgate et al., 2000). The approximate stratigraphic locations of the Mount Isa (MI), Hilton (HI), George Fisher (GF), Lady Loretta (LL), and Century (CE) Zn-Pb-Ag deposits are denoted by asterisks. In the Mount Isa area, the Gun and Loretta supersequences are represented by the Mount Isa Group, which is subdivided into the upper and lower Mount Isa Group with approximate formation thickness adapted from Neudert (1983).

Loretta deposits has been linked with dispersion of trace elements into seawater following hydrothermal venting (Lambert and Scott, 1973; Large et al., 2000; Large and McGoldrick, 1998). As a result, a number of element ratios and threshold values have been proposed to vector laterally towards CD-type massive sulphide systems in the Carpentaria province (Table 1).

One of the major caveats of existing alteration indexes is a sensitivity to compositional variability that is inherent to the host rock (Large et al., 2000). The challenge, therefore, is to develop alteration models that are able to discriminate between compositional heterogeneity that is inherent to background processes (authigenic, diagenetic, metamorphic) and those derived from hydrothermal input. In the deposits of the deformed Mount Isa Inlier, establishing a baseline protolith composition is complicated by (1) the varying degrees of tectonic overprint, (2) the lack of indicator minerals to constrain metamorphic grades, and (3) the enormous size of the mineralizing systems (e.g., Painter et al., 1999). These three aspects limit the availability of suitable correlative protolith lithologies, which are fundamental for developing geochemical and mineralogical exploration models.

In this study, we report bulk rock lithogeochemical and mineralogical data from (1) drill core samples through the main ore bodies at the

George Fisher deposit (165 Mt. at 9.1% Zn, 3.4% Pb, and 55 g/t Ag; JORC, measured and indicated resources, Glencore, 2019) and (2) from a correlative, barren drill core through mudstones and siltstones of the Urquhart Shale Formation (Shovel Flats drill-hole), which is the host rock to the George Fisher, Hilton (now mined in one operation with George Fisher) and Mount Isa deposits. We present a suite of compositional and mineralogical data using X-ray fluorescence (XRF; major elements), inductively coupled plasma mass spectrometry (ICP-MS, minor and trace elements), LECO (total organic carbon and sulphur) and X-ray diffraction (XRD; mineralogy) analyses. In combination with petrographic observations, we have evaluated the baseline lithological and compositional variability within the Urquhart Shale Formation and investigated the mass transfer and mineralogical transformations that may have been associated with ore formation and contributed to the alteration footprint in this part of the George Fisher deposit.

2. Geological background

2.1. Mount Isa Inlier, McArthur basin and superbasin cycles

The Mount Isa Inlier and McArthur Basin formed in an

intracontinental setting during the Paleo- to Mesoproterozoic (Fig. 1; Betts et al., 2016, Betts et al., 2002; Giles et al., 2002). Basin formation was initiated during the late Paleoproterozoic (ca. 1790 Ma) and was followed by several episodes of rifting, sag phases and inversion, which are recorded by sedimentary rocks that can be separated into 3 unconformity bound superbasin sequences (Leichhardt Superbasin, Calvert Superbasin and Isa Superbasin; Gibson et al., 2016; Giles et al., 2002; Southgate et al., 2000). Basin closure then corresponded with the onset of the Isan orogeny (ca. 1600 Ma; Page et al., 2000).

Based on lithostratigraphic and chronostratigraphic correlations, these superbasin sequences are further subdivided into 12 correlated supersequences (e.g., Jackson et al., 2000; Page et al., 2000; Southgate et al., 2013). The Calvert and Isa Superbasins, which host the Mount Isa, George Fisher – Hilton, Lady Loretta, McArthur River and Century deposits, consist of the Big and Prize supersequences (Calvert Superbasin; Southgate et al., 2013; Southgate et al., 2000) and the Gun, Loretta, River, Term, Lawn, Wide and Doom Supersequences (Isa Superbasin; Southgate et al., 2013, Southgate et al., 2000). In the Mount Isa area, there has been debate over whether the host rocks to the Mount Isa and George Fisher – Hilton deposits (Fig. 2; Gun Supersequence) belong to the Isa Superbasin (Southgate et al., 2013, Southgate et al., 2000) or to the Calvert Superbasin (Gibson et al., 2016).

2.2. Mount Isa group

The Mount Isa Group comprises a series of fine-grained, clastic sedimentary rock formations that belong to both the Gun and Loretta supersequences (Fig. 2b). Sedimentation was interpreted to have occurred during transgressive and highstand conditions on a gently inclined shelf in the Leichhardt River Fault Trough, which resulted in deposition of siliciclastic and carbonate facies (Southgate et al., 2013). The formations of the Mount Isa Group can be further separated into the Lower and Upper Mount Isa Group by an unconformity between the Breakaway Shale and the Native Bee Siltstone (Fig. 2; Mathias and Clark, 1975; van den Heuvel, 1969). There is an overall decrease in grain size through the Lower Mount Isa Group, with near-shore deposition of conglomerates and sandstones of the Warrina Park Quartzite transitioning to finer-grained deeper water siltstones and mudstones of the Moondarra Siltstone and Breakaway Shale (Derrick, 1974; Domagala et al., 2000; Mathias and Clark, 1975; Neudert, 1983). The Upper Mount Isa Group (Fig. 2b) is composed mainly of siltstones and mudstones, which are mostly thinly bedded and comprise dolomite, quartz, K-feldspar, albite, muscovite, phlogopite and chlorite with minor calcite, pyrite, siderite, tourmaline, zircon, rutile and carbonaceous matter (Neudert, 1983).
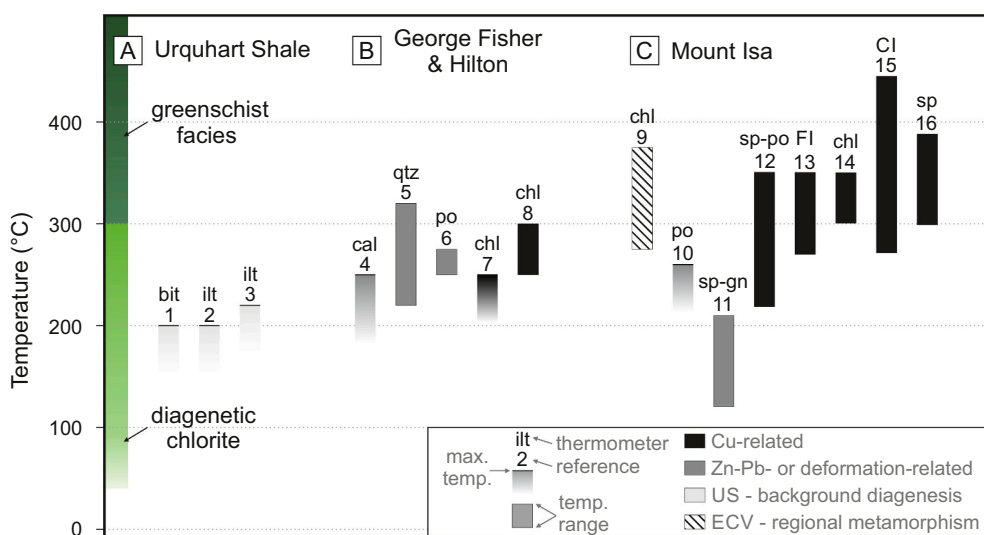

Fig. 3. Temperature constraints for (A) the Urquhart Shale Formation, (B) the George Fisher and Hilton deposits, and (C) the Mount Isa deposit. The green bars indicate temperatures of diagenetic chlorite formation and of greenschist facies metamorphic conditions. Individual temperature constraints are derived from: (1) bitumen reflectance (Chapman, 1999), (2) illite crystallinity (McClay, 1979), (3) maximum burial temperature derived from clay fraction analysis (this study), (4–6) calcite twinning, fractal analysis of quartz and from pyrrhotite twinning (Murphy, 2004), (7) alteration associated with Cu-mineralization derived from chlorite stability (Chapman, 2004), (8) alteration associated with Cu-mineralization derived from chlorite stability (Valenta, 1988), (9) regional metamorphism in the Eastern Creek Volcanics derived from chlorite-quartz isotopic equilibrium (Hannan et al., 1993), (10) crystal structure of pyrrhotite (van den Heuvel, 1969), (11−12) temperature of Zn-Pb and Cu mineralization derived from sphalerite-galena and sphalerite-pyrrhotite S-isotope equilibrium respectively (Painter et al., 1999), (13) fluid inclusion homogenization temperatures in Cu mineralization (Heinrich et al., 1989), (14) chlorite alteration associated with Cu-mineralization (Waring, 1990), (15) clumped isotopes in carbonates associated with Cu-mineralization (Mering et al., 2018), and (16) sphalerite thermometry (Cave et al., 2020). Temperature constraints are grouped by their relationship to regional metamorphism (Eastern Creek Volcanics), diagenesis (Urquhart Shale), Zn-Pb mineralization, deformation, or Cu-mineralization. (For interpretation of the references to colour in this figure legend, the reader is referred to the web version of this article.)

2.3. Urquhart Shale formation

The Urquhart Shale Formation mostly comprises laminated to bedded siltstones and mudstones and has a gradational contact with the underlying Native Bee Siltstone Formation and the overlying Spear Siltstone Formation (Bennett, 1965; Neudert, 1983). The Urquhart Shale is siliceous to dolomitic, variably pyritic and carbonaceous and can generally be distinguished from the Native Bee Siltstone and Spear Siltstones by a much higher abundance of pyrite (Neudert, 1983). The depositional ages of the Urquhart Shale Formation at the Mount Isa and George Fisher-Hilton deposits have been determined via U-Pb dating of zircons from interbedded tuff beds (1652 ± 7 Ma and 1654 ± 5 Ma respectively; Page et al., 2000; Page and Sweet, 1998).

Several sedimentary facies have been identified in the Urquhart Shale Formation, which have generally been linked to sabkha or playa environments and emergent to semi-emergent conditions in the lower Urquhart Shale and a more distal, carbonate slope to basin environment in the upper Urquhart Shale (Neudert, 1983). Further facies analysis refined this model and identified three dominant sedimentary facies in the Urquhart Shale Formation (Painter et al., 1999; Painter, 2003): (1) a rhythmite facies, comprising fining-upwards sequences of inter-laminated mudstones and siltstones, with abundant nodular carbonates as pseudomorphs after sulphate evaporites in the siltstones; notably, this facies comprises the bulk of the Zn-Pb mineralization at the Mount Isa deposit; (2) a carbonate cemented siltstone facies, which consists mostly of barren, massive calcareous and dolomitic siltstones with minor mudstones; and (3) cross-laminite facies, comprising cross-laminated siltstones and fine sandstones with minor mudstones. Based on these sedimentary facies, the overall depositional environment of the Urquhart Shale was interpreted to resemble sedimentation on a carbonate slope proximal to a saline mudflat or sabkha environment (Painter, 2003). Alternatively, sedimentary features, which were previously interpreted to represent evaporitic processes (e.g., nodular carbonates), were interpreted as diagenetic precipitates and overall the Urquhart Shale was considered to have been deposited as rhythmites in a deeper water environment (Domagala et al., 2000).

Previous lithogeochemical studies on the Urquhart Shale Formation have focused on drill core samples from between the Mount Isa deposit and the Transmitter Fault (Painter, 2003; Fig. 2). The Urquhart Shale is generally depleted in silicate-associated elements (Si, Al, Ti, Na, ± K) and enriched in carbonate-associated elements (Ca, Mg, Mn, ± Fe) relative to Post-Archean-Australian-Shale (PAAS; Nance and Taylor, 1976). Late diagenetic Zn-Pb mineralization has resulted in the enrichment (Mn, Fe, Pb, Zn, Ag, Tl, Ge, S, Cd, As, and Sb), depletion (Ca, Mg, Na, and Sr), and dilution (Si, Ti, Al, K, Zr, and Y) of several elements from un−/weakly-mineralized Urquhart Shale to the Mount Isa deposit. Based on these element changes, an alteration vector was formulated, which results in increasing values towards the Mount Isa deposit (Isa vector; Table 1). Furthermore, the mineralogical changes towards the Mount Isa deposit were reported to be preserved by higher abundances of sulphide (pyrite, sphalerite, galena, and pyrrhotite) and ferromanganese carbonate minerals (dolomite and ankerite) relative to un−/ weakly-mineralized Urquhart Shale.

2.4. Deformation and metamorphism of the western Mount Isa Inlier

The Mount Isa Inlier has been affected by multiple stages of deformation and varying degrees of metamorphism (Blake, 1987). During the Isan orogeny (ca. 1610 to 1510 Ma), polystage deformation resulted in folding and faulting, and peak metamorphic conditions (sub-greenschist to amphibolite facies) have been constrained to the first phase of *E*-W compression (Bell and Hickey, 1998; Connors and Page, 1995; Page and Bell, 1986). In the Mount Isa and George Fisher area, the highest metamorphic grades (greenschist to amphibolite facies) are located west of the Mount Isa – Paroo Fault Zone and east of the Sybella batholith (ca. 1670 Ma; Connors and Page, 1995; Page and Bell, 1986; Wyborn et al.,

1988). In the uppermost section of the Eastern Creek Volcanics, which are located in the footwall of the Paroo Fault at the Mount Isa deposit, temperatures of 325 °C ± 50 °C were reached during regional metamorphism (temperature derived from the isotopic equilibrium of quartz and chlorite; Hannan et al., 1993). There is a sharp contrast in metamorphic grade (amphibolite to sub-greenschist conditions) from uplifted rocks west of the Mount Isa – Paroo Fault zone to the sedimentary rocks of the Mount Isa Group in the east of the fault zone, where a lack of metamorphic indicator minerals complicate the determination of metamorphic grades (Valenta, 1994). The only proposed metamorphic indicator minerals in the Mount Isa Group are chlorite (Rubenach, 1992; Wilson, 1972) and stilpnomelane (Heinrich et al., 1989), which would indicate lower greenschist metamorphic conditions. Chlorite is also part of the alteration assemblage associated with high temperature Cu-mineralization at George Fisher, Hilton, and Mount Isa (Fig. 3; Cave et al., 2020; Chapman, 1999; Valenta, 1988; Waring, 1990). There are fewer temperature constraints for the un-mineralized Urquhart Shale Formation, but bitumen reflectance and illite crystallinity indicate maximum burial temperatures of ca. 200 °C (Chapman, 1999; McClay, 1979), which are significantly lower than greenschist metamorphic conditions (≥300 °C; Fig. 3).

2.5. George fisher deposit

The George Fisher deposit is located approximately 20 km north of Mount Isa (Fig. 2). The ore bodies are hosted by mudstones and siltstones of the Urquhart Shale Formation. There are 9 ore domains (A to I, Fig. A1), which are further subdivided into un-mineralized domains of barren mudstones and siltstones, weakly mineralized domains, and the main Zn-Pb ore bodies. Multiple generations of sulphides have been described at the George Fisher deposit (Chapman, 1999, 2004; Murphy, 2004; Rieger et al., 2020a), which are broadly sub-divided into (0) fine-grained pyrite, (1) stratabound sphalerite + pyrite ± galena, (2) breccia-hosted galena + sphalerite + pyrite + pyrrhotite and (3) vein and breccia-hosted pyrite + pyrrhotite + chalcopyrite ± galena and sphalerite.

There are different genetic models for the mineralization at George Fisher. For example, Murphy (2004) interpreted structural and paragenetic data to suggest that most of the mineralization formed *syn*-tectonically during the latest of four major deformation events (D4; equivalent to D3 event described by Bell and Hickey, 1998) at temperatures of 200–300 °C (Fig. 3). In contrast, a combination of paragenetic data, Pb-model ages, and metal distributions have been interpreted to support a model in which the bulk of the Zn-Pb mineralization at George Fisher and Hilton formed syn-diagenetically and pre-deformation, with Cu (± Zn-Pb) mineralization linked to a later hydrothermal event (e.g., Chapman, 2004; Chapman, 1999; Valenta, 1994). The latter model is supported by more recent work that reported in situ sulphur isotope analyses of pyrite (Rieger et al., 2020a), which interpreted: 1) formation of fine-grained pyrite by microbial sulphate reduction during early diagenesis (pre-ore); 2) stratabound Zn mineralization (ore stage 1) during burial diagenesis with S derived from thermochemical sulphate reduction (TSR), and; 3) later Zn-Pb (ore stage 2) and Cu (ore stage 3) mineralization, with reduced sulphur derived from recycling of earlier sulphides and TSR. Precise constraints for the timing of individual ore forming events are, however, lacking and structural observations can be interpreted in support of a variety of relative timings (cf. contrasting interpretations by Chapman, 1999, 2004; and Murphy, 2004). Nonetheless, there is general agreement that Cu-mineralization at the George Fisher deposit is paragenetically late and was associated with the highest temperature hydrothermal event (see references in Fig. 3).

Multiple phases have been linked to alteration at the George Fisher deposit, including ferroan dolomite, quartz, K-feldspar, pyrite, hydrophlogopite, and Ba(-K)-feldspar (Chapman, 1999, 2004). Zones of intense Ba(-K)-feldspar alteration were reported in the deeper parts of the deposit and Ba was interpreted to be derived from the hydrothermal
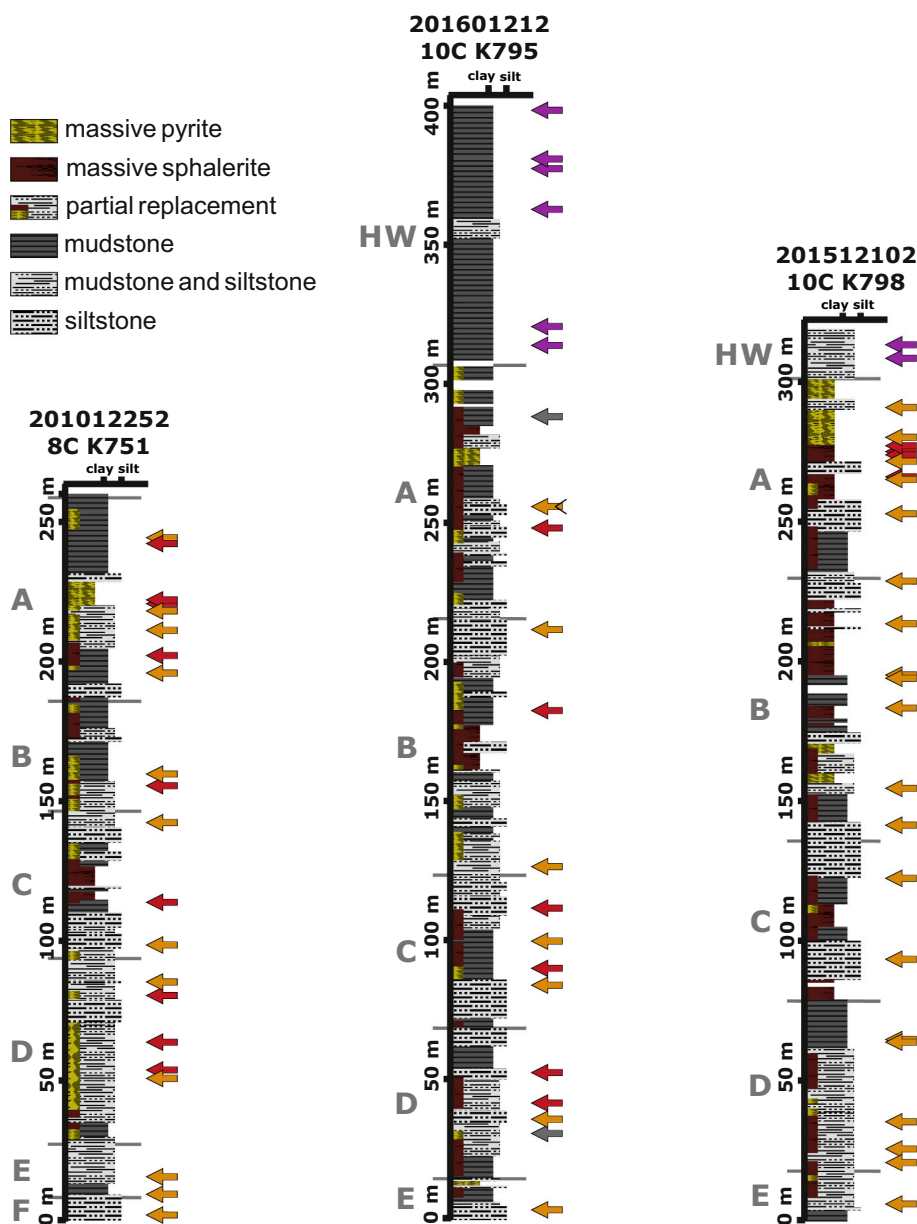
Fig. 4. Lithological logs of drill cores 8C K751, 10C K795 and 10C K798 from the George Fisher deposit. The drill-holes were drilled from east to west (stratigraphically old to young) and intersected mine nomenclature domains A-F (grey labels; George Fisher operations, Mount Isa Mines). The samples analysed in this study are hanging wall Urquhart Shale (purple), inter-mineralization Urquhart Shale (orange) and massive sulphides (red). (For interpretation of the references to colour in this figure legend, the reader is referred to the web version of this article.)

fluid (Chapman, 1999). In contrast, Painter (2003) suggested that Ba-feldspar formed due to diagenetic replacement and pseudomorphism of carbonate and feldspar after barite in the un-mineralized Urquhart Shale near Mount Isa. Later syn-tectonic Cu-mineralization at George Fisher was associated with siderite, ferroan ankerite, biotite, chlorite, muscovite and magnetite alteration (Chapman, 1999, 2004). Unlike other deposits of the Carpentaria Province (e.g., Lady Loretta, Large and McGoldrick, 1998; McArthur River, Large et al., 2000 Mount Isa, Painter, 2003; Century, Whitbread, 2004) there has been no previously published investigation of the bulk rock lithogeochemistry at George Fisher.

3. Methods and samples

3.1. Sampling and petrography

A total of 91 representative samples were selected from the Shovel Flats drill core, which intersects ca. 900 m of the un-mineralized Urquhart Shale Formation (Figs. 2 and A2). A total of 225 samples

were taken from 4 drill-holes that intersected the main ore bodies at the George Fisher deposit (8C K751, $n = 61$; 10C K795, $n = 77$; 10C K798, $n = 57$; 12C I797, $n = 30$). Samples from the George Fisher deposit comprise representative examples from the main ore bodies, from weakly mineralized sections, and from barren siltstones and mudstones between the ore bodies, and the hanging wall stratigraphy. Particular emphasis was given to sampling from drill-hole 10C K795, as it preserves 300 m of stratigraphy through the domains A-E and 100 m through un-mineralized hanging wall Urquhart Shale (Fig. 4).

Petrographic examination of the samples was conducted using a desktop binocular microscope and key samples ($n = 90$) were selected for transmitted light and reflected light microscopy. A subset of 41 representative samples from the background drill-hole and 70 representative samples from the George Fisher deposit were then selected for X-ray diffraction and lithogeochemical analyses. Where possible, sampling was targeted to individual lithologies and for each sample a sub-sample of ca. 30 g was taken.
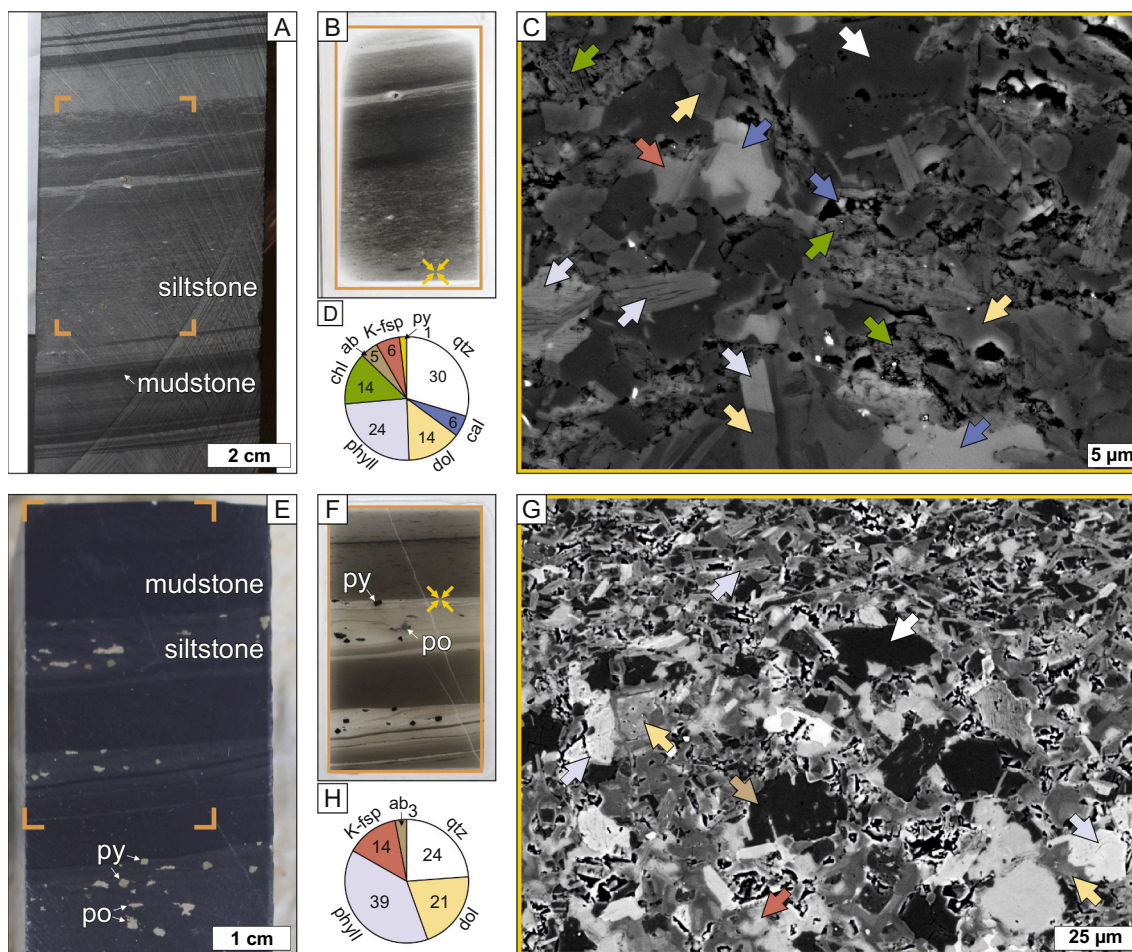
Fig. 5. A–D. Interbedded mudstone and siltstone (sample PR832SF012) from Shovel Flats drill core. A. Hand specimen photograph with mudstone (dark) and siltstone (grey); the orange rectangle indicates location of B. B. Thin section photograph with mudstone and siltstone; the yellow arrows indicate the location of C. C. Backscatter electron (BSE) image of siltstone; the arrows indicate individual mineral phases, see D for colour code. D. Bulk-rock XRD mineralogical composition (qtz = quartz, cal = calcite, dol = dolomite, phyll = 10 Å-phyllosilicate, chl = chlorite, ab = albite, K-fsp = K-feldspar, py = pyrite). 5*E*-H. Interbedded mudstone and siltstone (sample PRK7952001) from George Fisher drill core 10C K795. E. Hand specimen photograph with mudstone (dark) and siltstone (grey) with pyrite and pyrrhotite; the orange rectangle indicates location of F. F. Thin section photograph with carbonaceous mudstone and dolomitic siltstone; the yellow arrows indicate the location of G. G. BSE image of dolomitic siltstone; the arrows indicate individual mineral phases, see H for colour code. H. Bulk-rock mineralogical composition (qtz = quartz, dol = dolomite, phyll = 10 Å-phyllosilicate, K-fsp = K-feldspar, ab = albite). (For interpretation of the references to colour in this figure legend, the reader is referred to the web version of this article.)

3.2. Bulk rock lithogeochemistry and mineralogy

The samples were crushed and powdered to a grain size of <62 μm and whole rock geochemical analysis was carried out by Bureau Veritas Minerals (BVM) in Vancouver, Canada. Major, minor and trace element concentrations were analysed by ICP-MS of lithium borate fused rock powders. Trace metal concentrations (Mo, Cu, Pb, Zn, Ni, As, Cd, Sb, Bi, Ag, Au, Hg, Tl, and Se) were determined by ICP-ES/MS of aqua regia digested rock powders (upper detection limit for Zn and Pb = 10,000 ppm). Lithium borate fused samples with over limit Zn and Pb concentrations were analysed by X-ray fluorescence. Concentrations of total S, total C, C_{org} (organic carbon), C_{gra} (graphitic carbon), and CO_2 were determined by a LECO analyser. Low total concentrations in some samples are due to incomplete combustion of sulphide minerals. In addition to internal measures (duplicates, blanks, and reference materials) for assessing accuracy and precision of the analyses at BVM, blanks (quartz sand) and blind reference materials were routinely run for data quality control. Analyses of the SBC-1 ($n = 7$) reference material (USGS) had median uncertainties of 1.2% for element oxides and of 2.4% for trace elements for certified values; median uncertainties for recommended values for ShBOQ-1 (USGS; $n = 12$) were 1.3% and 4.2% for

element oxides and trace elements respectively. Median uncertainties for certified values were 1.0% and 2.3% for the massive sulphide standards (ORE Research & Exploration Pty Ltd) OREAS 131a ($n = 3$) and OREAS 134a (n = 3) respectively.

Quantification of the bulk rock mineralogical composition was determined using a PANalytical Empyrean X-ray diffractometer (GFZ Potsdam). Splits of the lithogeochemistry samples were further homogenized to <10 μm with a micronizing mill. The measurements were performed at 40 mA and 40 kV with CuKα radiation and a step size of 0.013°2Θ with 60s/step from 4.6 to 75°2Θ. The mineralogy was determined with the EVA software (version 11.0.0.3) by Bruker. Rietveld refinement for quantitative mineralogy was performed using the program BGMN and the graphical user interface Profex (Doebelin and Kleeberg, 2015) calibrated for the used diffractometer. The uncertainty of the quantitative analyses is ≤3 wt% for individual phases. High Pb and Zn concentrations in 7 samples resulted in overlapping signals between sphalerite and galena with carbonate mineral phases (calcite and dolomite) during Rietveld refinement resulting in an overestimation of carbonate concentrations (the mineralogical composition of these samples is not reported). To determine the pyrite abundance of these samples, Pyrite abundance was calculated on the basis of molar fractions of
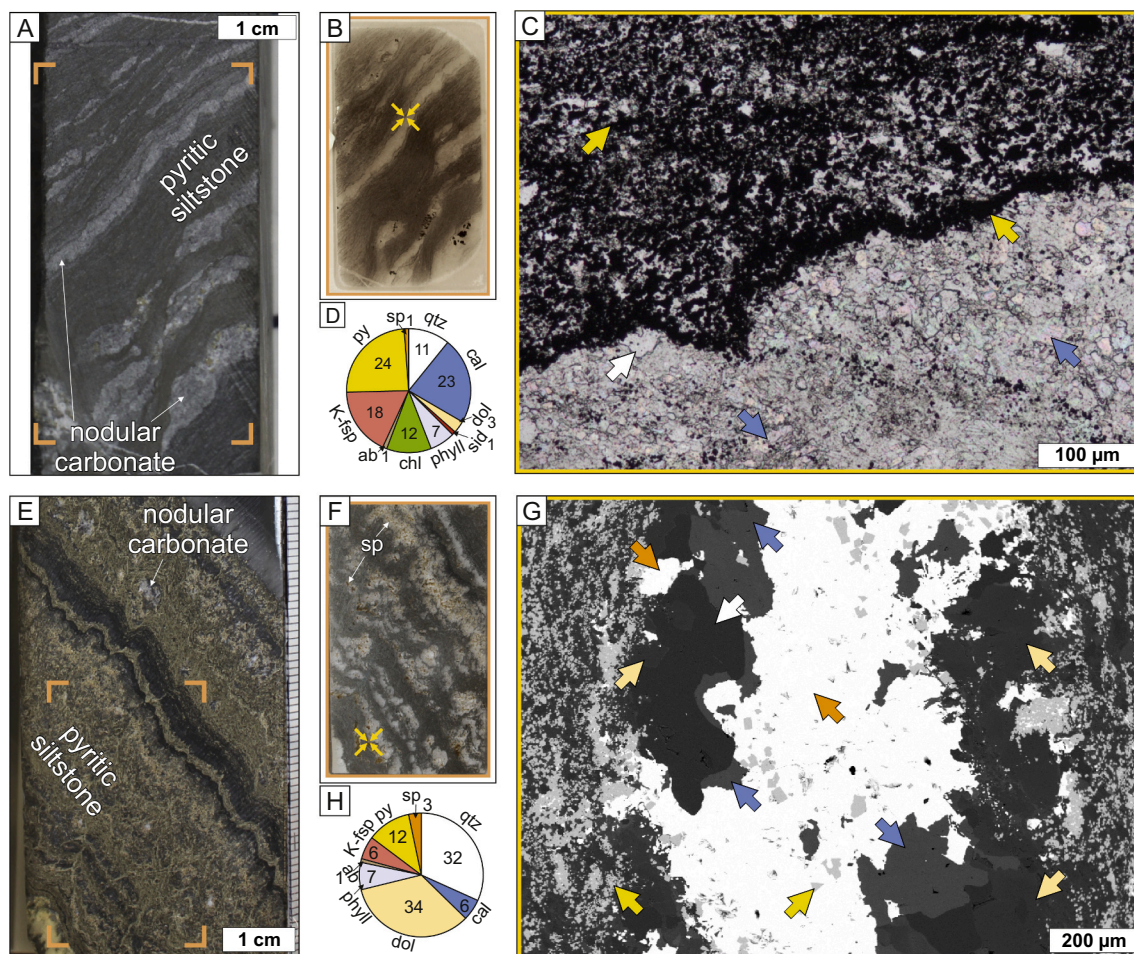
Fig. 6. Nodular carbonate and pyritic siltstone samples (Shovel Flats A-D, sample PR832SF080; George Fisher E-H, sample PRK751017). A. Hand specimen photograph; the orange rectangles indicates location of B. B. Thin section photograph of nodular carbonate and pyritic siltstone; the yellow arrows indicate the locations of C. C. Transmitted light photomicrograph of nodular carbonate and pyritic siltstone; the arrows indicate individual mineral phases, see D. for colour code. D. Bulk-rock mineralogical composition (qtz = quartz, cal = calcite, dol = dolomite, sid = siderite, phyll = 10 Å-phyllosilicate, chl = chlorite, ab = albite, K-fsp = K-feldspar, py = pyrite, sp. = sphalerite). E. Hand specimen photograph; the orange rectangles indicates location of F. F. Thin section photograph of nodular carbonate and pyritic siltstone; note sphalerite in nodular carbonates; the yellow arrows indicate the locations of G. G. Backscatter electron image of sphalerite replacing nodular carbonate; the arrows indicate individual mineral phases, see H. for colour code. H) Bulk-rock mineralogical composition (qtz = quartz, cal = calcite, dol = dolomite, phyll = 10 Å-phyllosilicate, ab = albite, K-fsp = K-feldspar, py = pyrite, sp. = sphalerite). (For interpretation of the references to colour in this figure legend, the reader is referred to the web version of this article.)

S, Pb, and Zn from the lithogeochemistry dataset. Therefore, sphalerite- and galena-bound S was subtracted from total S; these S values were then used to calculate the total S and Fe contained in pyrite. The clay-size (< 2 μm) fraction of Shovel Flats (n = 10) and George Fisher samples (n = 7) was prepared from separate rock chips that were mechanically crushed and separated following the analytical methods described by (Moore and Reynolds Jr, 1997). Air-dried and ethylene-glycol solvated oriented mounts were scanned from 2° to 35° at 0.01°2Θ intervals.

3.3. Statistical analysis

The Gresens' method was used to quantify mass change between un-altered and altered samples. This analysis is based on the calculation of the *isocon*, which is defined by the ratio of immobile elements in the altered rock relative to its un-altered equivalent (Grant, 1986). As summarised by Grant (2005), this ratio of immobile elements can be determined by using (1) the clustering of element ratios (concentration $_{altered}$ / concentration $_{un-altered}$), (2) a best fit line (*isocon* line) through the origin and immobile elements in an *isocon* diagram (Grant, 1986), (3) the pre-selection of immobile elements, or (4) the assumption of constant mass or constant volume during alteration processes.

For the graphical presentation of this method, major, minor and trace element concentrations have to be arbitrarily scaled in order to plot on one graph. As a result of arbitrary scaling the apparent distance of an element to the *isocon* is strongly dependent on the scaling factor (Humphris et al., 1998). To eliminate this scaling effect, a modified *isocon* diagram can be formulated by consistently scaling all the data to plot on a circle with distance of 1 to the origin (sums of squares of each element = 1; Humphris et al., 1998). In this modified *isocon* diagram, groups of elements that behave similarly (e.g., immobile elements) will group together on one segment of the circle. This may simplify the selection of immobile elements in order to define the *isocon* (zero mass change).

After determination of the immobile elements, the bulk mass loss or gain (ΔM, in percent) of the altered rock relative to the un-altered rock can be calculated using (e.g., Wilkinson et al., 2011):

$$\Delta M = 100 * \left[\frac{c_{i\_altered} - c_{i\_un-altered}}{c_{i\_altered}} \right]$$

where $c_{i\_altered}$ and $c_{i\_un-altered}$ are the concentrations of one or multiple immobile elements in the altered and un-altered rock respectively.
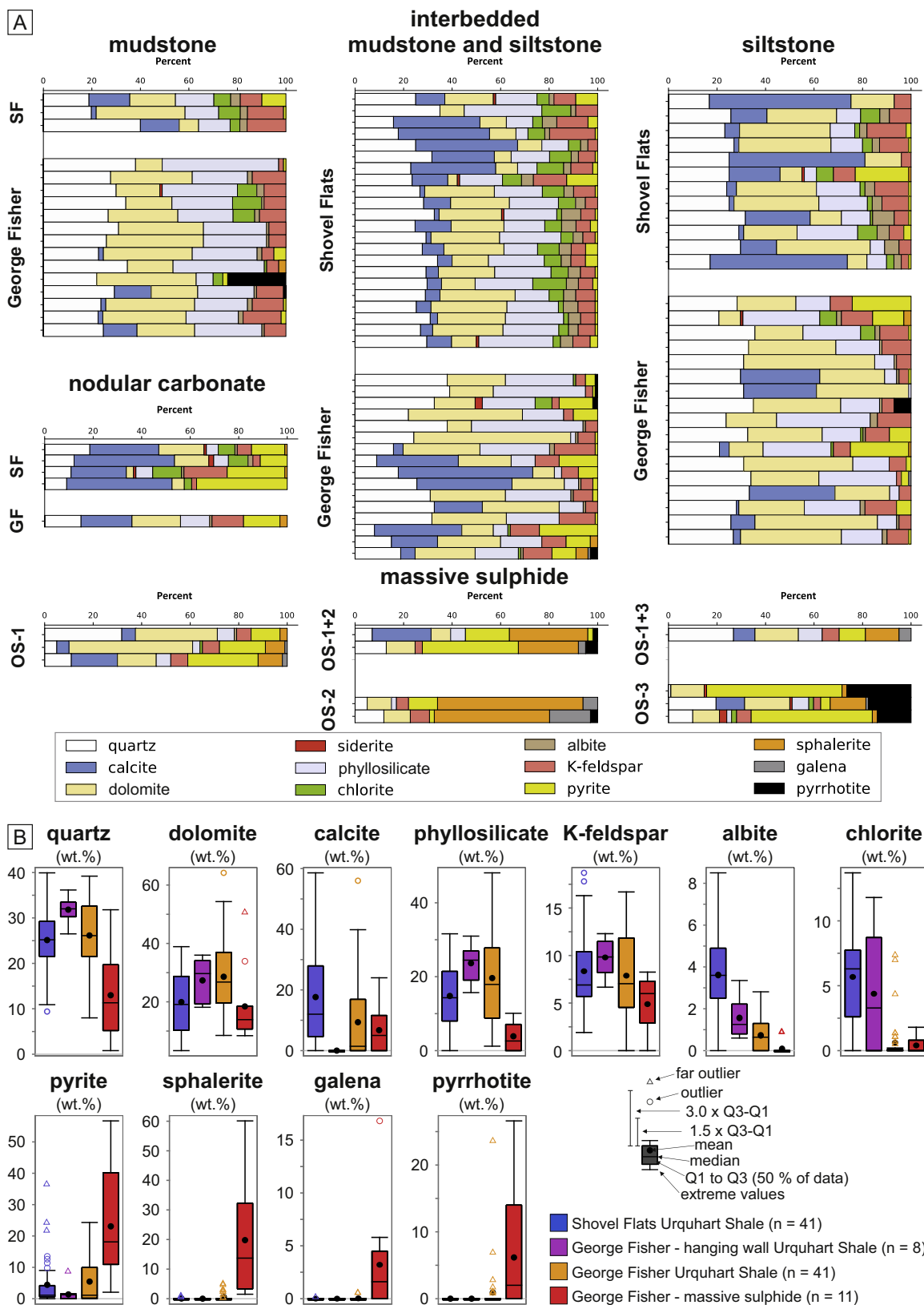
Fig. 7. Mineralogical composition of samples from the Shovel Flats drill core and the George Fisher deposit. A. Bar plot of individual samples split by lithology. B. Box and whisker plots for individual mineral phases are split by location. Also shown are the statistical details of the box and whisker plots used in this study.
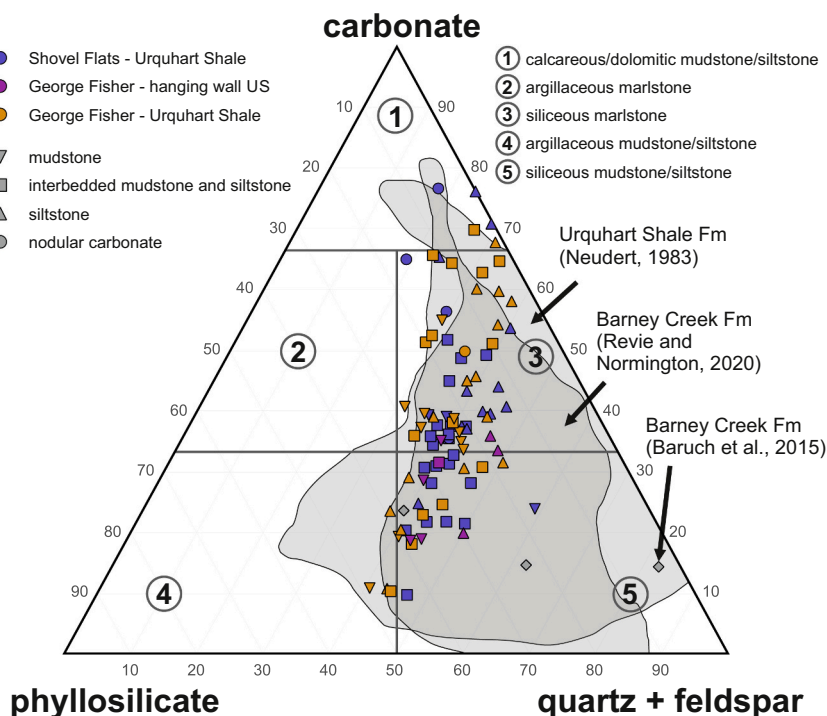
Fig. 8. Ternary diagram of three main mineral groups (carbonate, phyllosilicate and quartz + feldspar) plotting individual samples from the Shovel Flats drill core and from the George Fisher deposit and literature data for the Urquhart Shale Formation (Neudert, 1983) and the Barney Creek Formation (Baruch et al., 2015; Revie and Normington, 2020).

Furthermore, the addition or loss of an element (ΔE, in percent) in the altered sample relative to the un-altered sample is given by:

$$\Delta E = 100 * \left[\frac{c_{altered}}{\left(\frac{c_{i\_altered}}{c_{i\_un-altered}} \right) * c_{un-altered}} - 1 \right]$$

where $c_{altered}$ and $c_{un-altered}$ are the concentrations of an element in the altered and un-altered sample respectively.

In this study the immobile elements were determined by combining the modified graphical approach developed by Humphris et al. (1998) and the clustering of element ratios (Grant, 2005). Only elements that group together using both methods for both precursor sub-groups were considered immobile, which was further evaluated using the chemical index of alteration (Nesbitt and Young, 1982). Immobile element ratios were then used to calculate median values, mean values and standard deviations for the *isocon*. To account for any compositional heterogeneity inherent to the un-mineralized Urquhart Shale samples, only elements with a slope greater or smaller than two standard deviations of the *isocon* were considered to be either enriched or depleted at the George Fisher deposit. To avoid overestimation of median values by removing below detection limit data, these data were imputed as 0.5 * detection limit values (e.g., Na₂O, detection limit = 0.01 wt%, value imputed for data below detection limit = 0.005 wt%).

4. Results

4.1. Lithological logs

The Shovel Flats drill core preserves a long section of un-mineralized Urquhart Shale Formation (ca. 900 m). The upper 300 m of the drill-hole intersected a deep regolith profile and only 300 to 900 m are shown in Fig. A2. The Urquhart Shale Formation primarily comprises interbedded mud- and siltstone (Fig. 5) with intervals of massive siltstone, and thinner intervals of more homogenous mudstone, siltstone, or nodular carbonate. Nodular carbonate beds, which are typically ≤10 cm thick, are not resolved at the scale of logging (Fig. A2), and are typically interbedded with pyritic carbonaceous siltstones (Fig. 6). The carbonate nodules are up to several cm in the lateral dimension and ≤2 cm thick. The samples preserve no well-developed foliation or deformation fabric at the hand specimen or thin section scale, although there has been some localized deformation associated with discrete fractures or small shear zones.

The drill-holes from the George Fisher deposit intersected lithologies that are comparable to those from the Shovel Flats drill core (Fig. 4). The Urquhart Shale Formation between the intervals of massive sulphide mainly comprises interbedded mud- and siltstones and intervals with more homogeneous mudstones, siltstones, or nodular carbonates. In all 4 drill cores, the ore stage 1 mineralization is stratabound in mostly laminated, carbonaceous siltstones and in nodular carbonates. Subsequent ore stage 2 and 3 mineralization is more independent of lithology and commonly crosscuts several individual lithologies in massive ore breccias or ore veins. There is a minor fault followed by 100 m of hanging-wall stratigraphy to ore domain A preserved in drill core 10C K795, which consists mostly of homogeneous mudstone.

4.2. Mineralogy

4.2.1. Shovel flats samples

The main mineral phases (median ≥ 1 wt%) in Urquhart Shale samples from the Shovel Flats drill core are quartz, calcite, dolomite, 10 Å-phyllosilicates (muscovite, phlogopite, illite), chlorite, albite, K-feldspar, and pyrite (Fig. 7). The samples can be grouped according to mineralogical endmembers of (1) carbonates, (2) quartz and feldspars, and (3) phyllosilicates (muscovite, phlogopite, illite, and chlorite), which then corresponds with a rock type classification of calcareous/dolomitic mudstones and siltstones, siliceous marlstones and siliceous mudstones and siltstones (Fig. 8).

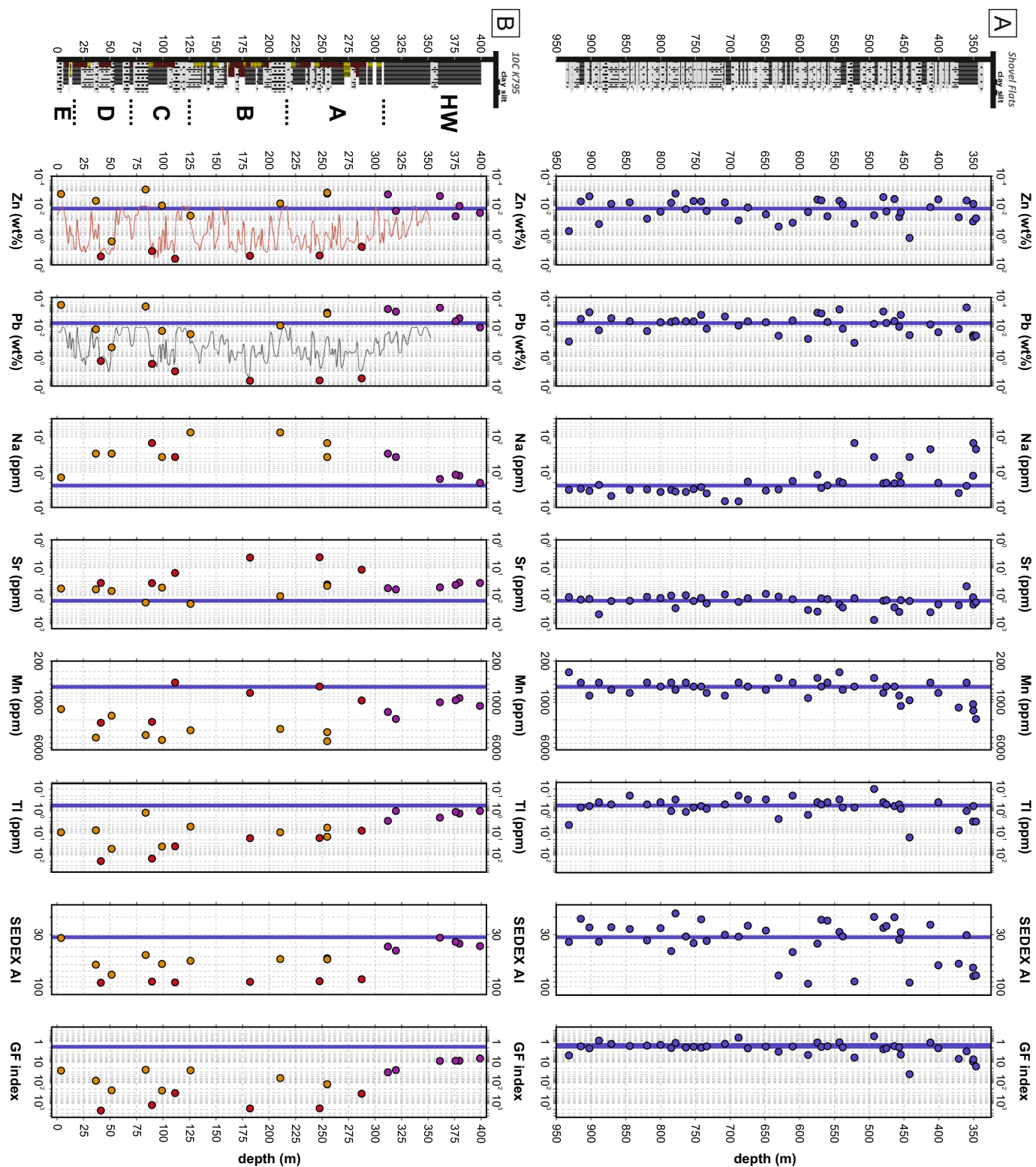Chlorite typically occurs as clay-sized particles together with fine-

Fig. 9. Chemostratigraphic logs for the Shovel Flats drill core (A) and for drill core 10C K795 from the George Fisher deposit (B) with the downhole variation of Zn, Pb, Na, Sr, Mn, Tl, SEDEX alteration index values and the George Fisher Index $(10[400Tl + Mn]/[10Sr + Na])$. Zinc and Pb plots include mine assay data (red line = Zn; grey line = Pb). The blue lines show the median values of individual element of Urquhart Shale samples from Shovel Flats. The samples in B. are grouped by colour: red = massive sulphide; orange = inter-mineralization Urquhart Shale; purple = hanging wall Urquhart Shale. (For interpretation of the references to colour in this figure legend, the reader is referred to the web version of this article.)
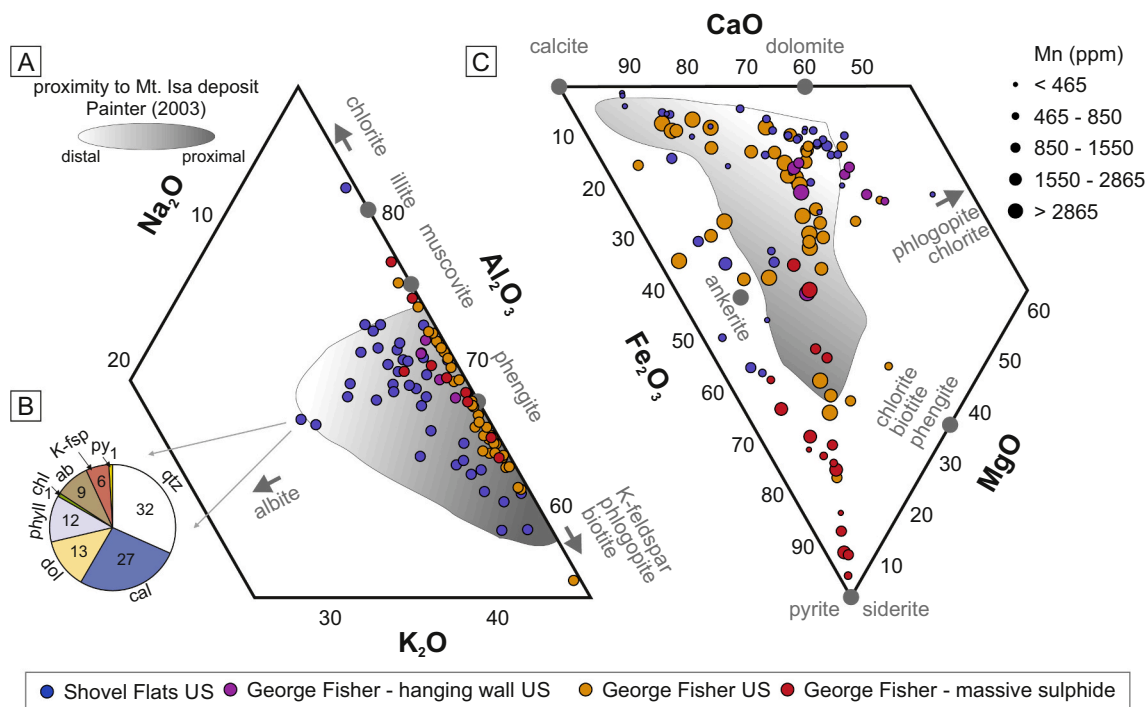
Fig. 10. A. Na₂O, K₂O and Al₂O₃ ternary diagram for samples from the Shovel Flats drill core and the George Fisher deposit. End-member compositions of selected mineral phases are shown in grey. The grey field represents Urquhart Shale samples distal (white) to proximal (dark grey) to the Mount Isa deposit (data from Painter, 2003). B. Bulk-rock mineralogical composition of sample PR832SF035 from the Shovel Flats drill core (qtz = quartz, cal = calcite, dol = dolomite, phyll = 10 Å-phyllosilicate, chl = chlorite, ab = albite, K-fsp = K-feldspar, py = pyrite). This sample preserves the highest albite content in the XRD data set. C. CaO, MgO and Fe₂O₃ ternary diagram for samples from the Shovel Flats drill core and the George Fisher deposit. End member compositions of selected mineral phases are shown in grey. The grey field represents Urquhart Shale samples distal (white) to proximal (dark grey) to the Mount Isa deposit (data from Painter, 2003).

grained illite in interstitial pore spaces in silicate and carbonate minerals (Fig. 5). Most Shovel Flats samples contain relatively low abundances of pyrite (< 5 wt%), although high concentrations (< 37 wt%) are preserved in some samples of nodular carbonate interbedded with laminated carbonaceous siltstones.

4.2.2. George Fisher samples

The un-mineralized samples from between the ore bodies at the George Fisher deposit contain similar proportions of the main mineral groups to the samples from Shovel Flats (Figs. 7 and 8). In contrast, the samples from the hanging wall stratigraphy in 10C K795 generally preserve higher and lower abundances of silicate and carbonate minerals respectively. The abundances of quartz, K-feldspar and pyrite are relatively consistent between the Shovel Flats samples and those from the George Fisher deposit. Compared to the Shovel Flats samples, dolomite and 10 Å-phyllosilicate phases are more abundant in the George Fisher samples, whereas calcite, chlorite and albite are less abundant to absent (Figs. 7 and 8).

Massive sulphide samples from George Fisher preserve higher abundances of all sulphide minerals and generally lower abundances of all other minerals, the only exception being higher median calcite contents compared to George Fisher Urquhart Shale samples (Fig. 7).

4.2.3. Clay-fraction mineralogy of the Urquhart Shale Formation (Shovel Flats and George Fisher)

The main difference in the clay fraction mineralogy between the two groups of samples (Shovel Flats and George Fisher) is the absence of chlorite in most of the George Fisher samples. Illite has been identified in the <2 μm clay size fraction in all samples from Shovel Flats and George Fisher, based on the peak position, the peak shape and the peak height of the 001 basal reflection in the oriented clay mounts (Fig. A3), and the

hkl polytypes 1Md and 2 M1 in the bulk rock samples. Compared to the Shovel Flats samples, the shape of the 001 basal reflections of illite in the George Fisher samples is indicative of a possible transition of the 10 Å-phyllosilicates from illite to muscovite (Fig. A3) and the asymmetric peak shape in some samples indicates that very little illite-smectite remains. The same results are produced when the samples are treated with ethylene glycol, which indicates there is little smectite in the samples.

4.3. Bulk rock geochemistry

The bulk rock compositional data of all samples is presented in Rieger et al. (2020b) and the chemostratigraphic logs for some of the key analytes are presented in Fig. 9.

4.3.1. Major element and base metal composition

Most samples from George Fisher contain very little Na and plot between Al and K in a ternary diagram of these 3 components, whereas samples from Shovel Flats preserve a similar range of K/Al ratios but plot towards higher Na concentrations (Fig. 10A). The samples from George Fisher that are located in the hanging wall sequence to massive sulphide mineralization are intermediate between the two groups (Fig. 10A). In terms of Ca, Mg and Fe concentrations, samples mostly plot between the calcite, dolomite, and pyrite end-members (Fig. 10C). In comparison to Shovel Flats, the George Fisher samples contain elevated Mn and the sub-group from the ore lenses plot towards the Fe end-member (Fig. 10C).

Base metal concentrations and total S can vary between the ore stages (Fig. 11A-D). Samples from ore stage 2 contain the highest Zn and Pb concentrations; ore stages 1 and 3 contain relatively lower Zn and Pb but are still highly enriched relative to un-mineralized samples from George Fisher and Shovel Flats (Fig. 11A-D). In contrast, samples from
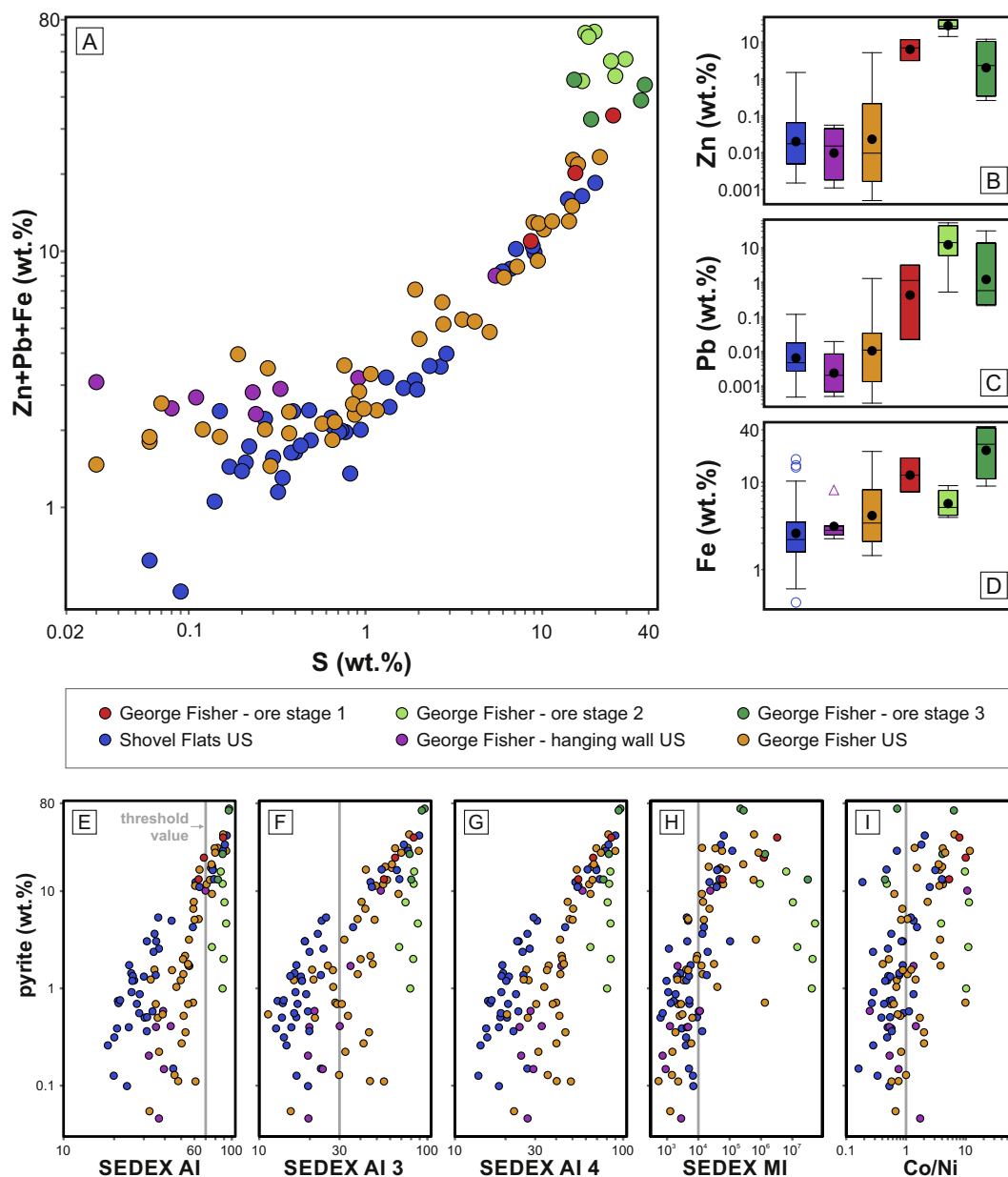
Fig. 11. A.-D. Sulphur and base metal concentrations for samples from the Shovel Flats drill core and the George Fisher deposit. A. Sulphur vs. combined Zn-Pb-Fe. B. Box and whisker plot for Zn concentrations. C. Box and whisker plot for Pb concentrations. D. Box and whisker plot for Fe concentrations. For details of the statistical method for box and whisker plots see Fig. 7B. E.-I. Literature alteration indexes vs. pyrite abundance for samples from the Shovel Flats drill core and the George Fisher deposit. E. SEDEX alteration index. F. SEDEX alteration index mark 3. G. SEDEX alteration index mark 4. H. SEDEX metal index. I. Cobalt/Ni ratio.

Shovel Flats and the un-mineralized samples from George Fisher have broadly overlapping total S and base metal concentrations. In the 10C K795 drill core at George Fisher, the Zn and Pb concentrations of the Urquhart Shale samples from the hanging wall and from in between the ore bodies are scattered around the median concentrations from the Shovel Flats drill core. In terms of alteration indexes, the values for the SEDEX AI, SEDEX AI 3, SEDEX AI 4, the SEDEX metal index and the Co/Ni ratio are highest in the massive sulphide samples (Fig. 11E-I). A total of 21 of the 41 Shovel Flats samples are below the suggested threshold values for CD-type massive sulphide deposits in the Carpentaria province (Table 1). Ten samples are above threshold values for less than four of these indices and another 10 samples are above threshold values for four or more indexes. All samples with pyrite contents of more than 10 wt% fall into this category (Fig. 11). Molybdenum concentrations are generally low (Fig. 12; 62 samples <2 ppm; 39 samples 2 to 10 ppm; 4

samples 10 to 25 ppm).

4.3.2. Comparing shovel flats and George Fisher samples

The Shovel Flats samples ($n = 21$) that have below threshold values for the SEDEX alteration indexes were used as a reference for the un-altered protolith composition of the Urquhart Shale. The samples were further subdivided into two groups according to lithology: (1) siltstones ($n = 9$) and (2) mudstone and interbedded mudstone-siltstones ($n = 12$).

To evaluate relative mass changes, and element losses and gains median values for major, minor, and trace elements of each sub-group were compared (Fig. 13). The ratios of the immobile elements (Si, Al, Ti, Sc, Nb, Th, Y, and REE) in both lithological subgroups preserve evidence of a small bulk mass loss (ΔM) of 2% (siltstones) and 4% (combined mudstones and siltstones) in the George Fisher samples (relative to un-altered Shovel Flats samples). The largest element gains (> 50%)
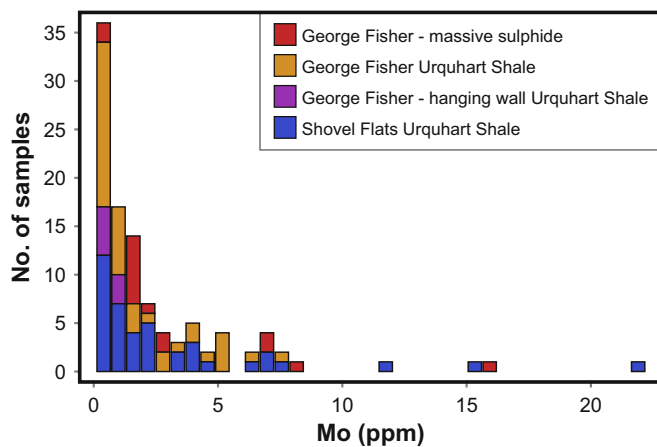
Fig. 12. Molybdenum concentrations for samples from the Shovel Flats drill core and the George Fisher deposit (bin width = 0.6 ppm).

are Tl, Ag, Mn, S, Pb; Fe and Cu for the siltstones, and Zn and Co for combined mudstones and siltstones. Cobalt, Zr, Mo, and Hf are moderately enriched (50% to 2 standard deviations of *isocon* line) in the siltstones, and Fe and K are moderately enriched in combined mudstone and siltstone samples respectively.

There is a large depletion (>50%) in Na, Sr and C_{gra} for both lithological sub-groups, and for Zn and Cs in siltstones. Barium, Mg and Ni are moderately depleted (50% to 2 standard deviations of *isocon* line) in both sub-groups; Cs, Sb, and Cu in the combined mudstones and siltstones, and; U, CO_2, C_{org}, P, Ca, As and C_{tot} in the siltstones.

Overall, the bulk mass loss and the enrichment or depletion factors of the most enriched or depleted elements (e.g., Tl, Mn, Ag, Na, Sr) and the immobile elements (Si, Al, Ti, Sc, Nb, Th, Y, and REE) are similar for both lithology sub-groups (Fig. 13A, B, E). For comparison with the massive sulphide samples from the George Fisher deposit, both lithologies for un-altered samples (n = 21) from the Shovel Flats drill core were combined to identify the most enriched and most depleted elements (Fig. 13C, D).

The bulk mass change ($\Delta M = 100 * \left[\frac{c_{i\_GF} - c_{i\_SF}}{c_{i\_GF}} \right]$) of the massive sulphide samples relative to the un-altered Urquhart Shale samples indicates a large mass gain of 283%. Chalcophile (Cd, Zn, Pb, Ag, Hg, Tl, S, Sb, Se, As, Cu) and siderophile elements (Co, Fe, Mo) are strongly enriched (>1000%). Furthermore, Mn and Ni are enriched (> 500–1000%) and TOC and Eu are slightly enriched (500% to 2 standard deviations of *isocon* line) in the massive sulphide samples relative to the background Urquhart Shale samples. Element depletion (>2 standard deviations of *isocon* line) is indicated for Na, C_{gra}, Sr, Ta, V, and P. Overall, the elements, which show the greatest variability between the Shovel Flats drill-hole and the George Fisher deposit are Zn, Pb, Na, Mn, Sr, and Tl (Fig. 9).

4.3.3. George Fisher index

The elements for which there is the greatest difference between Shovel Flats and George Fisher (Zn, Pb, Na, Mn, Sr and Tl) are all relatively uniform in total concentration in the Shovel Flats samples (Fig. 9). The one exception is in the uppermost 200 m, where concentrations of Mn and Tl are slightly elevated and Na and Sr are present at slightly lower concentrations. This variability also corresponds with scatter in the SEDEX AI values.

The non-base metal elements within this sub-group (Na, Mn, Sr and Tl) have been used to formulate an alteration index for the George Fisher deposit (GF Index). Element factors have been applied to obtain 1:1 proportion between Tl and Mn, and between Sr and Na for the Urquhart Shale samples, *i.e.* $10 \left(\frac{400Tl + Mn}{10Sr + Na} \right)$. The Shovel Flats samples preserve the

lowest index values (median = 1.9), although they are slightly elevated in the upper 100 m of the drill core. The GF Index is highest in the mineralized samples from George Fisher, whereas the un-mineralized samples have intermediate values (Fig. 14). Overall, the GF Index provides improved sensitivity for differentiating between the sample subgroups (Fig. 14) when compared to the existing SEDEX AI's (Fig. 11).

There is a negative correlation between Sr and Mn, whereby the highest Sr/Ca ratios and lowest Mn/Ca ratios are preserved in Shovel Flats samples and lowest Sr/Ca ratios and highest Mn/Ca ratios in George Fisher samples (Fig. 15). Thallium concentrations covary strongly with pyrite abundance and Tl/pyrite ratios (ppm/wt%) are generally high in Urquhart Shale and ore stage 1 and 2 samples at George Fisher and low in Shovel Flats samples and samples from ore stage 3 (Fig. 16). Similarly, Ag concentrations covary with pyrite abundance and preserve elevated Ag/pyrite ratios for all George Fisher samples relative to Shovel Flats. Notably, the highest Ag/pyrite values are preserved by ore stage 2 samples, which also preserve the highest concentrations of Zn and Pb (Fig. 11B, C).

5. Discussion

5.1. Unaltered composition of the Urquhart Shale Formation

It is essential to define the mineralogical composition of the unaltered protolith when developing accurate hydrothermal alteration models. For the George Fisher system, the unaltered protolith is represented by samples from the Shovel Flats drill-hole, which is located approximately 5 km away from the deposit (Fig. 2). The deposits in the northern Carpentaria Province are typically hosted within subbasins that represent localized fault-bound depocenters (e.g., Large et al., 2005), which preserve considerable lateral variability in the thickness and sedimentary facies of *syn*-tectonic depositional sequences (e.g., McGoldrick et al., 2010). In the Mount Isa Group there is similar evidence of syn-tectonic deposition in the form of variable formation thicknesses (e.g., Derrick, 1982; Smith, 1969). This sedimentological complexity makes precise stratigraphic correlations challenging to interpret, as correlative units may not necessarily preserve the same mineralogical constituents that then form the basis for subsequent alteration products. Moreover, this potential complexity has been further compounded by tectonic overprint in the southern Carpentaria (Valenta, 1994). Nevertheless, the Urquhart Shale samples from Shovel Flats, George Fisher (this study) and from the wider Mount Isa area (Neudert, 1983; Painter, 2003) do preserve overlapping detrital components (e.g., quartz and feldspars), authigenic components (e.g., diagenetic pyrite and carbonate), and 10 Å-phyllosilicate phases (e.g., muscovite, illite, and phlogopite) that justify this comparison (Fig. 5, 6, 7, and 8). These mineralogical similarities are further supported by overlapping major and trace element compositions (e.g., Figs. 10, 11, 12, and 15). Altogether, the mineralogy and geochemical composition of the Shovel Flats samples can be considered representative of the unaltered protolith to the George Fisher deposit and therefore as a baseline for evaluating alteration reactions.

Detrital constituents of sedimentary rocks represent the cumulative effect of a range of weathering, transport and depositional processes (Rimstidt et al., 2017) and provide the framework for all subsequent diagenetic reactions (Bjørlykke, 2014). During the Proterozoic it is generally accepted that low pO_2 limited terrestrial weathering to mostly physical processes, resulting in relatively immature siliciclastic input to sedimentary basins (Rafiei and Kennedy, 2019). The high abundance of feldspar in the Urquhart Shale is broadly similar to that described for the Barney Creek Formation in the McArthur Basin (Baruch et al., 2015), which is typical of chemically immature Precambrian sedimentary rocks (Kennedy et al., 2006). That said, the higher quartz/feldspar ratios in this study may imply a slightly different sediment source or deposition under deeper water conditions, which is consistent with the interpretation of deeper water rhythmite sedimentation for the Urquhart Shale
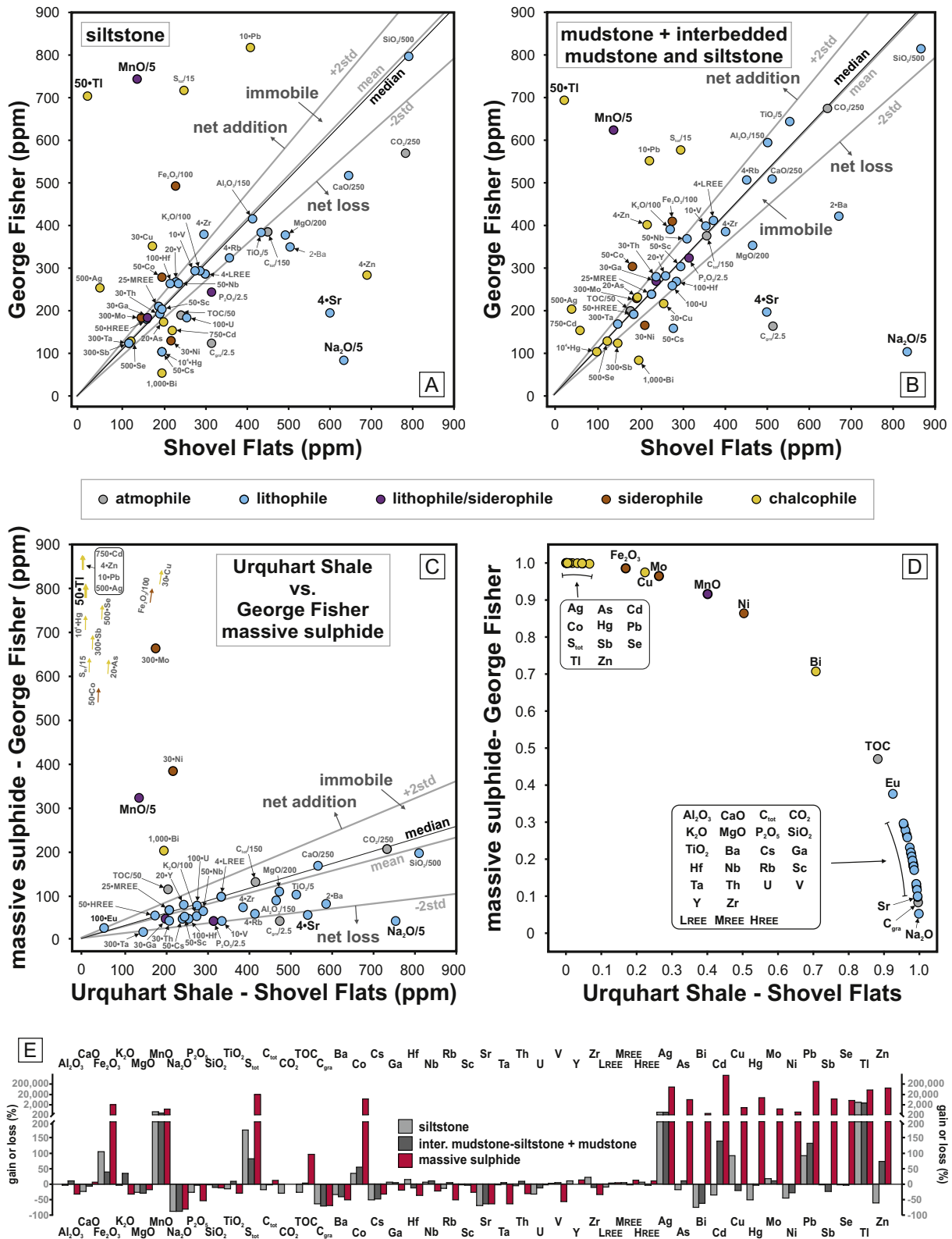
Fig. 13. Isocon diagrams for samples from the Shovel Flats drill core and the George Fisher deposit separated by lithology: A. Background (below alteration indexes) siltstone vs. George Fisher siltstone. B. Background (below alteration indexes) combined mudstone and mudstone-siltstone vs. George Fisher combined mudstone and mudstone-siltstone samples. C. Combined Background Urquhart Shale samples vs. George Fisher massive sulphide samples. D. Modified isocon diagram of C. with data scaled to a distance of 1 from the origin. Data in A.-C. are arbitrarily scaled to plot major and trace elements in a single diagram. A.-C. include the mean and median values and ± 2 standard deviation (2std) values for the isocon line defining a field of immobile behaviour. All elements are grouped according to their geochemical behaviour. E) Element mass gain and loss calculated for Shovel Flats vs. George Fisher samples shown in A.-D. for siltstone, combined mudstone and mudstone-siltstone, and for massive sulphide respectively.
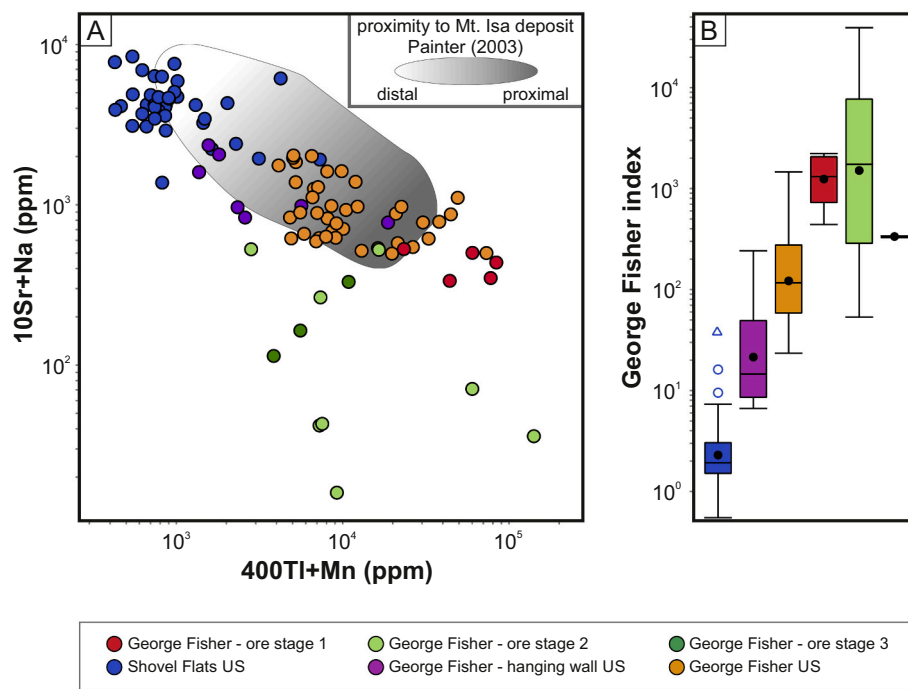
Fig. 14. George Fisher Index for samples from the Shovel Flats drill core and the George Fisher deposit. A. 400Tl + Mn vs. 10Sr + Na plot. The grey field represents Urquhart Shale samples distal (white) to proximal (dark grey) to the Mount Isa deposit (data from Painter, 2003). B. George Fisher index (10 (400Tl + Mn)/(10Sr + Na)) box and whisker plot. For details of the statistical method for box and whisker plots see Fig. 7B.
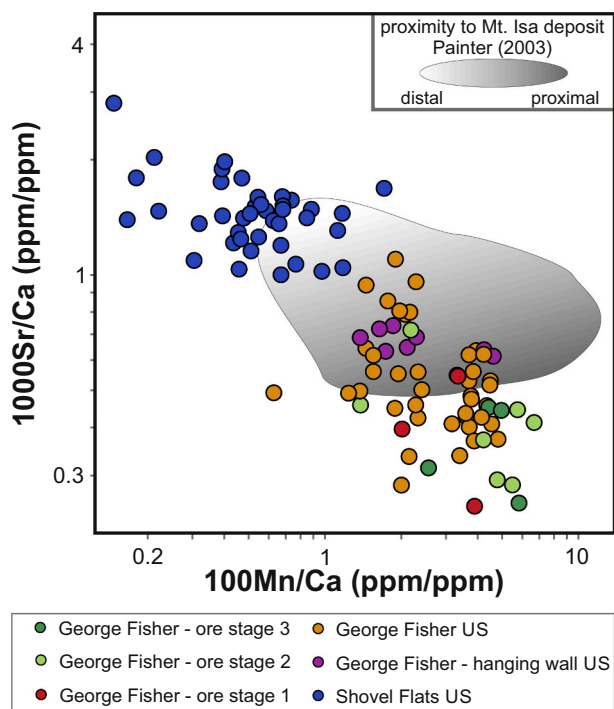

Fig. 15. Scatter plot of 100Mn/Ca vs. 1000Sr/Ca for samples from the Shovel Flats drill core and the George Fisher deposit. The grey field represents Urquhart Shale samples distal (white) to proximal (dark grey) to the Mount Isa deposit (data from Painter, 2003).

Formation (Domagala et al., 2000).

Biogenic and authigenic constituents in marine sediments are primarily associated with biological productivity in the water column and subsequent organic matter degradation during early diagenesis

(Rimstidt et al., 2017). The consumption of oxygen during oxygenic photosynthesis and subsequent organic matter degradation typically results in reducing depositional redox conditions. The interpretation of sulphur isotope values or Mo concentrations in sedimentary rocks can be used to reconstruct depositional and early diagenetic conditions in sedimentary basins. In unrestricted basins, for example, euxinic conditions ($H_2S > Fe^{2+}$) typically result in Mo concentrations (Mo >100 ppm; Scott and Lyons, 2012) that are enriched above crustal values (1–2 ppm; Taylor and McLennan, 1995). In Shovel Flats and George Fisher samples, low Mo concentrations (Fig. 12) indicate either a strong degree of water mass restriction or that euxinic conditions were not a widespread feature. Notably, the $\delta^{34}S$ values of fine-grained diagenetic pyrite (pre-ore) are consistent with open system conditions during microbial sulphate reduction (Rieger et al., 2020a), meaning that low levels of Mo enrichment could be explained by ferruginous conditions (i.e. $H_2S < Fe^{2+}$) during deposition of the Urquhart Shale Formation.

There is moderate enrichment of total organic carbon (TOC) in samples from the Urquhart Shale (1–2 wt%), which is similar to other Proterozoic fine-grained carbonaceous sedimentary rock units throughout the Carpentaria province (e.g., Baruch et al., 2015; Revie and Normington, 2020). With sufficient availability of organic matter and oxidants (e.g., sulphate, Fe-hydroxides, or Mn-oxides) microbial reactions during early diagenesis produce a number of reduced species (e.g., HS^-, Fe^{2+} and Mn^{2+}) and bicarbonate ions (HCO_3^-) and result in the formation of pyrite and carbonate. The formation of nodular carbonates in the Urquhart Shale is generally interpreted due to diagenetic processes (Domagala et al., 2000; Painter et al., 1999) and this is consistent with their pre-ore paragenetic timing at George Fisher (Fig. 6). As such, the pyrite and carbonate associated elements (Fe and S, and Ca, Mg, Sr, Mn and Fe respectively) in the un-mineralized Urquhart Shale are considered to largely represent biogenic and authigenic processes.

Phyllosilicate phases generally form in response to increasing pressures and temperatures during burial diagenesis (e.g., Bjørlykke, 2014; Rimstidt et al., 2017). These reactions involve the transformation of early diagenetic and detrital clay minerals (e.g., kaolinite, smectite)
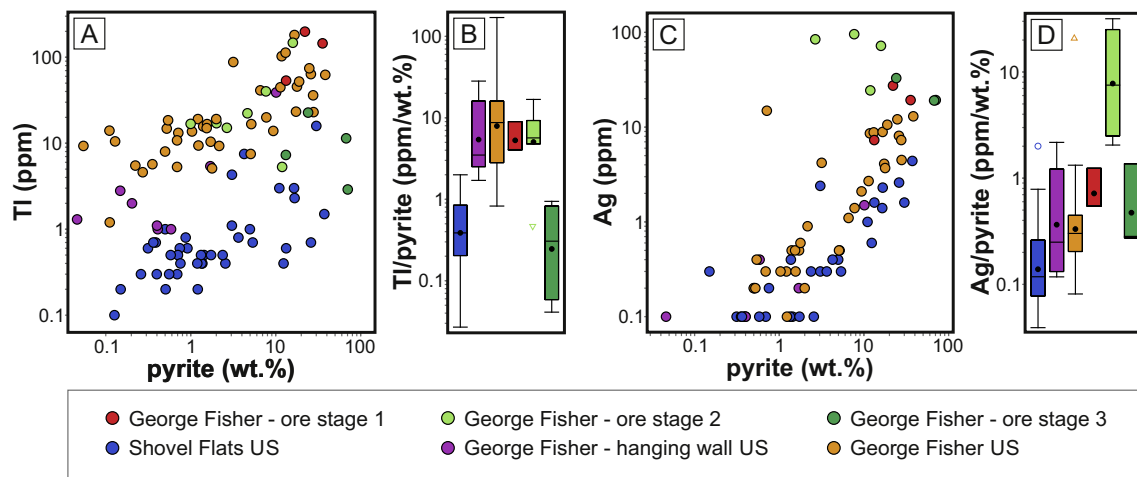
Fig. 16. A. Scatter plot of pyrite (wt%) vs. Tl (ppm) for samples from the Shovel Flats drill core and the George Fisher deposit. B. Box and whisker plot of the Tl/pyrite ratio. C. Scatter plot of pyrite (wt%) vs. Ag (ppm) for samples from the Shovel Flats drill core and the George Fisher deposit. D. Box and whisker plot of the Ag/pyrite ratio. For details of the statistical method for box and whisker plots see Fig. 7B.

through intermediate clay mineral phases, such as mixed-layered clay minerals (e.g., illite-smectite) and illite, to more crystalline phyllosilicate minerals such as muscovite or chlorite (e.g., Beaufort et al., 2015; Héroux et al., 1979; Lynch et al., 1997). The preservation of illite in the Urquhart Shale is consistent with sub-greenschist facies conditions (< 300 °C; Merriman and Frey, 1999). Moreover, asymmetric illite reflections may indicate the presence of very small amounts of illite-smectite interlayers (Fig. A3; see asymmetric illite-smectite reflections in Lanson and Besson, 1992; Lanson and Champion, 1991). Illite-smectite interlayers are not preserved above burial temperatures of 220 °C (Day-Stirrat et al., 2010), which is consistent with previous bitumen reflectance and illite crystallinity data from the Urquhart Shale (ca. 200 °C; Chapman, 1999; McClay, 1979).

Chlorite has previously been used as an indicator mineral for greenschist facies metamorphic conditions (> 300 °C) in the Urquhart Shale Formation and deposits of the Mount Isa area (Rubenach, 1992; Wilson, 1972; Large et al., 2005). In the un-mineralized Shovel Flats drill-hole, however, the preservation of illite (and illite-smectite; Fig. A3) and the absence of a well-developed metamorphic fabric are inconsistent with conditions of metamorphic chlorite formation. Rather, the fine-grained (<10 μm; Fig. 5 and A3) interstitial nature of chlorite in the Urquhart Shale Formation is consistent with diagenetic formation (e.g., Beaufort et al., 2015). It should be noted that the diagenetic chlorite is separate from the coarser grained chlorite that is more closely associated with Cu mineralization in a number of the deposits in the Mount Isa area (Cave et al., 2020; Chapman, 1999; Valenta, 1988; Waring, 1990).

The main pathways of diagenetic chlorite formation involve the transformation of precursor phases such as trioctahedral smectite or serpentine (e.g., berthierine; reaction (1); Beaufort et al., 2015).
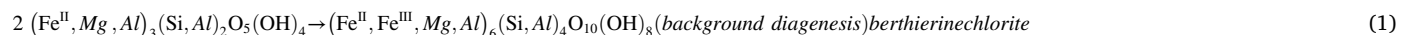
Virolle et al., 2019; Worden et al., 2020). It has also been suggested that under the ferruginous conditions that were characteristic of the Precambrian oceans, berthierine formation may have been widespread (e. g., Johnson et al., 2020; Tang et al., 2017). The diagenetic transformation of berthierine to chamosite (Fe-rich chlorite) is normally complete by 70 °C (e.g., Hornibrook and Longstaffe, 1996), meaning the chlorite in the Urquhart Shale Formation could have formed during burial diagenesis rather than metamorphism. Chlorite is also present in un-metamorphosed sedimentary rocks throughout the Tawallah, McArthur, Nathan, and Roper Groups of the McArthur Basin (Revie and Normington, 2020), which further supports such a diagenetic model for chlorite formation in the Proterozoic Carpentaria province.

5.2. Defining hydrothermal anomalism in the Urquhart Shale Formation

None of the published geochemical element ratios and alteration indices are particularly effective in differentiating between the Urquhart Shale Formation at the George Fisher deposit and the background Urquhart Shale Formation from the Shovel Flats drill core (Fig. 11). Covariation between pyrite abundance in the Shovel Flats samples and the SEDEX AI, SEDEX AI 3 and SEDEX AI 4 values indicates this alteration index is strongly dependent on pyrite abundance (Fig. 11). As there is considerable variability in background levels of pyrite (Rieger et al., 2020a), however, the SEDEX alteration indexes are susceptible to false positive values.

The SEDEX metal index values appear to be much more independent of pyrite abundance, although there is no clear differentiation between the background Urquhart Shale samples from the Shovel Flats drill core and the Urquhart Shale samples from the George Fisher deposit (Fig. 11). It is unlikely, therefore, that the ore forming metals are widely

$$2\left(\mathrm{Fe^{II}}, Mg, Al\right)_3(\mathrm{Si}, Al)_2\mathrm{O}_5(\mathrm{OH})_4 \rightarrow \left(\mathrm{Fe^{II}}, \mathrm{Fe^{III}}, Mg, Al\right)_6(\mathrm{Si}, Al)_4\mathrm{O}_{10}(\mathrm{OH})_8 (background\ diagenesis) berthierine chlorite \tag{1}$$

In modern estuarine and shelf environments berthierine formation has been linked to a suite of precursor phases (e.g., glauconite and odinite) formed from Fe-rich pore fluids during transgressive and highstand system tracts (e.g., Morad et al., 2010; Odin and Matter, 1981;
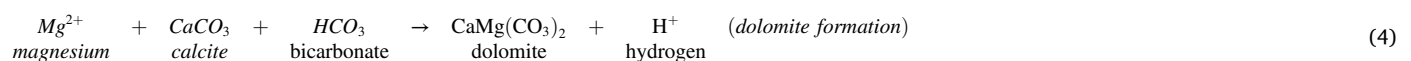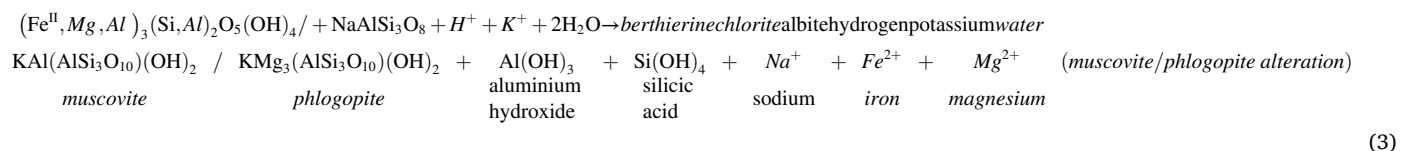
dispersed within the Urquhart Shale Formation at George Fisher. This lack of metal dispersion is consistent with the model of Zn ore formation in the sub-surface during diagenesis (Chapman, 1999, 2004; Rieger et al., 2020a) rather than the exhalation of the hydrothermal fluids on the seafloor.

In contrast, the GF Index discriminates between Urquhart Shale

samples from the background drill core, hanging wall samples from the George Fisher deposit, inter-mineralization Urquhart Shale samples and massive sulphide samples (Fig. 14). The elements in the GF Index are associated with the 3 major mineralogical constituents (silicates, carbonates, sulphides) of the Urquhart Shale Formation, meaning it is necessary to consider the alteration reactions involving these phases.

5.3. Hydrothermal alteration at George Fisher

The Cu-mineralization at the George Fisher deposit is a minor

and calcite during TSR (reaction (2)) would result in the formation of muscovite/phlogopite (reaction (3)), dolomite (reaction (4)) and pyrite (reaction (5)):

$$SO_4^{2-} + CH_4 \rightarrow HS + HCO_3 + H_2O \;\; (TSR)$$
$$\text{sulphate} \quad \text{methane} \quad \text{hydrogen sulphide} \quad \text{bicarbonate} \quad \text{water}$$

$$(2)$$

$$\left(Fe^{II}, Mg, Al\right)_3 (Si, Al)_2 O_5 (OH)_4 / + NaAlSi_3 O_8 + H^+ + K^+ + 2H_2O \rightarrow berthierine\, chlorite\, albite\, hydrogen\, potassium\, water$$

$$KAl(AlSi_3O_{10})(OH)_2 \; / \; KMg_3(AlSi_3O_{10})(OH)_2 + Al(OH)_3 + Si(OH)_4 + Na^+ + Fe^{2+} + Mg^{2+} \;\; (muscovite/phlogopite\ alteration)$$
$$\text{muscovite} \qquad\qquad \text{phlogopite} \qquad \text{aluminium hydroxide} \quad \text{silicic acid} \quad \text{sodium} \quad \text{iron} \quad \text{magnesium}$$

$$(3)$$

$$Mg^{2+} + CaCO_3 + HCO_3 \rightarrow CaMg(CO_3)_2 + H^+ \;\; (dolomite\ formation)$$
$$\text{magnesium} \quad \text{calcite} \quad \text{bicarbonate} \quad \text{dolomite} \quad \text{hydrogen}$$
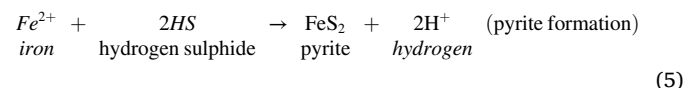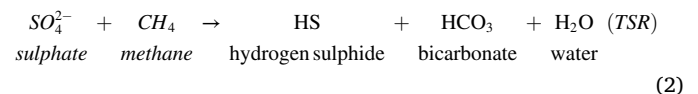
$$(4)$$

component and more spatially restricted than at the Mount Isa and Hilton deposits (Chapman, 1999). As such, the host rocks at the George Fisher deposit should preserve the geochemical footprint of the strata-bound Zn-Pb mineralization (ore stage 1) more effectively than the Mount Isa or Hilton deposits.

The greater abundances of dolomite and 10 Å-phyllosilicates at George Fisher relative to un-mineralized Shovel Flats samples (Fig. 7) are broadly comparable to previous alteration models (cf. Chapman, 1999, 2004). The main difference from earlier work is the absence of barium-(K-)feldspar, which was not detectable in any of the bulk rock mineralogical analysis. Furthermore, Ba is actually slightly depleted in mudstones and siltstones in George Fisher samples relative to Shovel Flats samples (Fig. 13). This may either indicate that (1) Ba-feldspar was dissolved or replaced during mineralization at George Fisher, or that (2) Ba-feldspar alteration was spatially restricted on a deposit scale. We consider (2) as being more likely, considering the observation that Ba-feldspar alteration is found mostly in the deeper parts of the deposit (Chapman, 1999). Such a model is perhaps similar to Ba-feldspar formation in the Irish-type Zn-Pb deposits, where Ba is introduced with the hydrothermal fluids and is incorporated into silicate minerals due to limited sulphate availability in the deeper parts of the systems (e.g., Riegler and McClenaghan, 2017).

The depletion of chlorite and albite in George Fisher samples relative to un-mineralized Shovel Flats samples (Fig. 7) has not previously been described. As discussed earlier, the un-mineralized host rocks to the George Fisher deposit likely contained diagenetic chlorite and is distinct from the hydrothermal chlorite that is more spatially restricted in association with the later Cu event (Fig. 7; Chapman, 1999). There are two options for the lack of chlorite in the George Fisher samples: (1) chlorite was never formed in the host rocks at George Fisher; or (2) hydrothermal processes have removed chlorite precursor phases (e.g., berthierine) or chlorite from the host rocks at the George Fisher deposit. There is no supporting evidence that protolith composition was substantially different in order to account for a contrasting diagenetic assemblage in the George Fisher samples (i.e. option 1). Instead, it is worth considering how alteration reactions involving the prograde diagenetic reaction sequence might control the mineralogical assemblage developed with ore stage 1. For example, the alteration of berthierine/chlorite, albite,

$$Fe^{2+} + 2HS \rightarrow FeS_2 + 2H^+ \;\; (pyrite\ formation)$$
$$\text{iron} \quad \text{hydrogen sulphide} \quad \text{pyrite} \quad \text{hydrogen}$$

$$(5)$$

This alteration reaction is consistent with the depletion of albite, chlorite, and calcite, and the greater abundances of muscovite/phlogopite and dolomite in samples from George Fisher (Fig. 7). The preservation of K-feldspar also suggests a high K^+/H^+ ratio in the fluid (relatively high pH), near the muscovite/K-feldspar stability boundary.

The magnesium released during berthierine/chlorite alteration (reaction (3)), combined with bicarbonate from TSR (II), could have resulted in hydrothermal dolomite formation (IV), which is consistent with the higher dolomite abundance at George Fisher relative to Shovel Flats Urquhart Shale samples (Fig. 7). Dolomitization of calcite typically results in changes in the trace element composition; for example, neo-formed dolomite is commonly enriched in Mn and/or Fe and depleted in Sr relative to precursor calcite (Brand and Veizer, 1980; Kah, 2000). These trace element changes are due to the incompatibility of the larger Sr^{2+}-ion compared to the smaller Mn^{2+}- or Fe^{2+}-ions in the dolomite structure (e.g., Kretz, 1982). The inverse relationship of Mn and Sr in Shovel Flats and George Fisher samples (Fig. 15) is consistent with hydrothermal dolomitization at the George Fisher deposit. Nodular carbonates at George Fisher also preserve evidence of replacement by sphalerite (Fig. 6; Chapman, 2004). The changes in whole rock carbonate mineralogy (calcite vs. dolomite) and replacement textures of dolomite by sphalerite likely indicate that mineralization has resulted in complex carbonate replacement and dissolution-precipitation reactions at George Fisher, although further studies on the carbonate chemistry are needed to test this hypothesis.

Reactive Fe from berthierine/chlorite (reaction (3)) and the hydrothermal fluid would have combined with reduced S (TSR; reaction (2)) to form hydrothermal pyrite (reaction (5)). Whole-rock Tl concentrations have previously been identified to be an important pathfinder for CD-type systems in the Carpentaria province (e.g., Lambert and Scott, 1973; Large and McGoldrick, 1998; Whitbread, 2004) and in other sedimentary basins (e.g., Gadd et al., 2016; Slack et al., 2004). Pyrite at George Fisher contains higher concentrations of Tl and Ag than pyrite
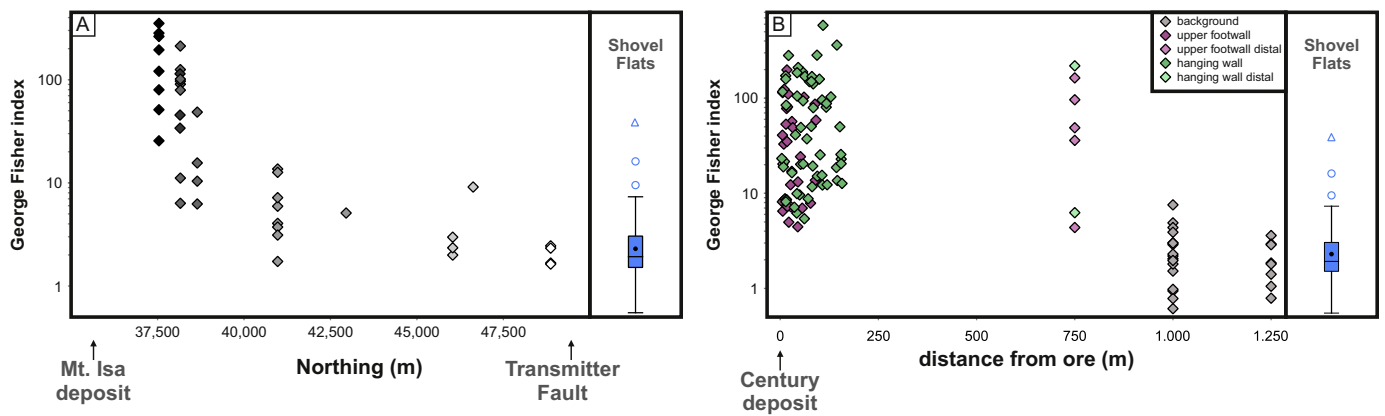
Fig. 17. George Fisher index values for the Urquhart Shale Formation north of the Mount Isa deposit (A; data compiled from Painter, 2003) and for the Century deposit (B; data compiled from Whitbread, 2004). George Fisher index values for the Shovel Flats samples (this study) are shown for reference.

from un-mineralized samples (Fig. 16). Recently, high-resolution element mapping of pyrite aggregates has shown that Tl-enriched pyrite formed after fine-grained pyrite in the McArthur River deposit (Spinks et al., 2019). At George Fisher, samples that are dominated by ore stage 1 preserve the highest whole rock Tl concentrations and have similar morphologies to McArthur River Tl-rich pyrites (Py-1; Rieger et al., 2020a). In contrast, the Tl/pyrite ratios of ore stage 3 (Cu-mineralization) are lower and are similar to background Urquhart Shale ratios (Fig. 16). Overall, the reaction sequence described by reactions (2)-(5) is consistent with lower chlorite albite, and calcite contents, higher 10 Å-phyllosilicate and dolomite abundances, and formation of hydrothermal pyrite at George Fisher and the element changes described by the GF index.

5.4. Implications

Considering the petrographic and mineralogical evidence that parts of the Urquhart Shale Formation did not reach greenschist facies (this study; Chapman, 1999; McClay, 1979) we argued above that the chlorite formed during diagenesis. It is possible, therefore, that compositional and isotopic data generated on samples from the Urquhart Shale Formation near the George Fisher deposit could be used to investigate the Paleoproterozoic depositional and diagenetic environment in this part of the Carpentaria province.

In terms of the sulphide mineralization at the George Fisher deposit, there is robust petrographic evidence that ore stage 1 (Zn-dominated, stratabound) post-dated the formation of diagenetic pyrite formed during the earliest stages of diagenesis (Rieger et al., 2020b). If so, it may have occurred either before, or after, diagenetic chlorite formation (i.e. < 70 °C, transformation of berthierine to chlorite). If the mineralization pre-dated diagenetic chlorite formation, this must have occurred within the upper 2–3 km of the basin (assuming a normal geothermal gradient). This is consistent with recent paragenetic models for mineralization at other deposits in the Carpentaria Province (e.g., Magnall et al., 2020). Alternatively, if ore stage 1 mineralization post-dated diagenetic chlorite formation, this may have occurred during late diagenesis (e.g., >3 km burial depth; cf. George Fisher, Chapman, 2004; Mount Isa, Painter, 2003). This would be consistent with ore formation models for the Century deposit, which likely formed during the onset of basin inversion (Broadbent, 2002; Broadbent et al., 1998). Notably, the depletion of albite and chlorite during hydrothermal activity has also been reported for the Century deposit (Whitbread, 2004).

Considering these mineralogical similarities, it is worth exploring the broader application of the GF index in the Carpentaria district. When applied to the Mount Isa and Century deposits the GF index can discriminate between the background protolith and the altered host rocks within approximately 2 km and 800 m of the respective deposits

(Fig. 17). Irrespective of the different paragenetic models that exist for the Carpentaria CD-type deposits, therefore, it is clear that alteration models should incorporate aspects of the sulphide, carbonate, and (phyllo)silicate assemblages; this will be most effectively achieved by combining petrographic, mineralogical, and bulk geochemical techniques.

6. Conclusions

The Urquhart Shale Formation is host to the world class George Fisher Zn deposit (165 Mt. at 9.1% Zn, 3.4% Pb, and 55 g/t Ag; Glencore, 2019) and consists of carbonaceous, variably dolomitic or calcareous siltstones and mudstones; un-mineralized mudstones and siltstones contain a variety of detrital and authigenic mineral phases (quartz, feldspars, phyllosilicates, calcite, dolomite, and pyrite). The occurrence of fine-grained chlorite in pores spaces with illite, the lack of well-developed metamorphic fabric, and low temperatures indicated by illite crystallinity are consistent with a sub-greenschist facies metamorphic grade. This implies that un-mineralized Urquhart Shale samples preserve a combination of detrital, authigenic and diagenetic components (including chlorite).

Hydrothermal alteration processes during ore stage 1 (Zn-dominated, stratabound) at the George Fisher deposit resulted in lower chlorite, albite, and calcite abundances, higher concentrations of dolomite and 10 Å-phyllosilicate minerals (e.g., muscovite or phlogopite), and the formation of sulphide minerals (pyrite, sphalerite, and galena). These mineralogical changes are consistent with a hydrothermal event either before, or after, the formation of diagenetic chlorite from berthierine. This may have occurred in the upper 2–3 km of the basin or during later diagenesis (e.g., at the onset of basin inversion). During this hydrothermal event, the dissolution of albite, the replacement of calcite by dolomite, and the formation of hydrothermal pyrite has resulted in minor and trace element depletion (Sr and Na) and enrichment (Tl and Mn), which were used to formulate an alteration index for the George Fisher deposit (GF index, $10\left(\frac{400Tl+Mn}{10Sr+Na}\right)$). This alteration index is highly effective in differentiating between the un-mineralized background Urquhart Shale Formation and the mineralized Urquhart Shale Formation at George Fisher. It may, therefore, be useful in future geochemical exploration programmes in the Mount Isa area. Moreover, similar mineralogical and element changes in other CD-type massive sulphide deposits may indicate that hydrothermal alteration reactions were broadly comparable throughout the Carpentaria province. Overall, the combination of petrographic, lithogeochemical, and mineralogical techniques has proved to be effective in determining the background composition of the Urquhart Shale Formation and the alteration footprint of the ore-forming system at George Fisher.

Declaration of Competing Interest

Acknowledgments

Appendix A. Supplementary data

Supplementary data to this article can be found online at https://doi.org/10.1016/j.chemgeo.2020.119975.

References

Aplin, A.C., Macquaker, J.H.S., 2011. Mudstone diversity: Origin and implications for source, seal, and reservoir properties in petroleum systems. Am. Assoc. Pet. Geol. Bull. 95, 2031–2059.

Baruch, E.T., Kennedy, M.J., Löhr, S.C., Dewhurst, D.N., 2015. Feldspar dissolution-enhanced porosity in Paleoproterozoic shale reservoir facies from the Barney Creek Formation (McArthur Basin, Australia). Am. Assoc. Pet. Geol. Bull. 99, 1745–1770.

Beaufort, D., Rigault, C., Billon, S., Billault, V., Inoue, A., Inoué, S., Patrier, P., Ferrage, E., 2015. Chlorite and chloritization processes through mixed-layer mineral series in low-temperature geological systems–a review. Clay Miner. 50, 497–523.

Bell, T.H., Hickey, K.A., 1998. Multiple deformations with successive subvertical and subhorizontal axial planes in the Mount Isa region; their impact on geometric development and significance for mineralization and exploration. Econ. Geol. 93, 1369–1389.

Bennett, E.M., 1965. Lead-zinc-silver and copper deposits of Mount Isa. Geol. Aust. Ore Depos. Mc Andrew, J. (Ed.), Eighth Commonw. Min. Metall. Congr. Melb. 2, 233–246.

Betts, P.G., Giles, D., Lister, G.S., Frick, L.R., 2002. Evolution of the Australian lithosphere. Aust. J. Earth Sci. 49, 661–695.

Betts, P.G., Armit, R.J., Stewart, J., Aitken, A.R.A., Ailleres, L., Donchak, P., Hutton, L., Withnall, I., Giles, D., 2016. Australia and nuna. Geol. Soc. London Spec. Publ. 424, 47–81.

Bjørlykke, K., 2014. Relationships between depositional environments, burial history and rock properties. Some principal aspects of diagenetic process in sedimentary basins. Sediment. Geol. 301, 1–14.

Blake, D.H., 1987. Geology of the Mount Isa inlier and environs, Queensland and Northern Territory. Austr. Bureau Min. Res. Bull. 225, 83.

Brand, U., Veizer, J., 1980. Chemical diagenesis of a multicomponent carbonate system; 1, Trace elements. J. Sediment. Res. 50, 1219–1236.

Broadbent, G., 2002. A decade of new ideas: Geology and exploration history of the Century Zn-Pb-Ag deposit, Northwestern Queensland, Australia. In Integrated methods for discovery: Global exploration in the twenty-first century. Econ. Geol. Spec. Publ. 9, 119–140.

Broadbent, G.C., Myers, R.E., Wright, J.V., 1998. Geology and origin of shale-hosted Zn-Pb-Ag mineralization at the Century deposit, Northwest Queensland, Australia. Econ. Geol. 93, 1264–1294.

Cave, B., Lilly, R., Barovich, K., 2020. Textural and geochemical analysis of chalcopyrite, galena and sphalerite across the Mount Isa Cu to Pb-Zn transition: implications for a zoned Cu-Pb-Zn system. Ore Geol. Rev. 103647.

Chapman, L.H., 1999. Geology and Genesis of the George Fisher Zn-Pb-Ag deposit Mount Isa, Australia. Unpubl. PhD Thesis. James Cook University, p. 315.

Chapman, L.H., 2004. Geology and mineralization styles of the George Fisher Zn-Pb-Ag deposit, Mount Isa. Australia. Econ. Geol. 99, 233–255.

Connors, K.A., Page, R.W., 1995. Relationships between magmatism, metamorphism and deformation in the western Mount Isa Inlier, Australia. Precambrian Res. 71, 131–153.

Day-Stirrat, R.J., Dutton, S.P., Milliken, K.L., Loucks, R.G., Aplin, A.C., Hillier, S., van der Pluijm, B.A., 2010. Fabric anisotropy induced by primary depositional variations in the silt: clay ratio in two fine-grained slope fan complexes: Texas Gulf Coast and northern North Sea. Sediment. Geol. 226, 42–53.

Derrick, G.M., 1974. Stratigraphic and palaeogeographic evolution and revolution in the Mount Isa area. In: Regional Meeting Pap Austra as Inst Min Metall NW Queensland Branch (Aug. 1974), pp. 177–187.

Derrick, G.M., 1982. A proterozoic rift-zone at Mount-Isa, Queensland, and implications for mineralization. BMR J. Aust. Geol. Geophys. 7, 81–92.

Doebelin, N., Kleeberg, R., 2015. Profex: a graphical user interface for the Rietveld refinement program BGMN. J. Appl. Crystallogr. 48, 1573–1580.

Domagala, J., Southgate, P.N., McConachie, B.A., Pidgeon, B.A., 2000. Evolution of the palaeoproterozoic prize, gun and lower loretta supersequences of the surprise creek formation and Mt Isa group. Aust. J. Earth Sci. 47, 485–507.

Eldridge, C.S., Williams, N., Walshe, J.L., 1993. Sulfur isotope variability in sediment-hosted massive sulfide deposits as determined using the ion microprobe SHRIMP; II, a study of the HYC Deposit at McArthur River, Northern Territory, Australia. Econ. Geol. 88, 1–26.

Gadd, M.G., Layton-Matthews, D., Peter, J.M., Paradis, S.J., 2016. The world-class Howard's Pass SEDEX Zn-Pb district, Selwyn Basin, Yukon. Part I: trace element compositions of pyrite record input of hydrothermal, diagenetic, and metamorphic fluids to mineralization. Mineral. Deposita 51, 319–342.

Gibson, G.M., Meixner, A.J., Withnall, I.W., Korsch, R.J., Hutton, L.J., Jones, L.E.A., Holzschuh, J., Costelloe, R.D., Henson, P.A., Saygin, E., 2016. Basin architecture and evolution in the Mount Isa mineral province, northern Australia: Constraints from deep seismic reflection profiling and implications for ore genesis. Ore Geol. Rev. 76, 414–441.

Gibson, G.M., Hutton, L.J., Holzschuh, J., 2017. Basin inversion and supercontinent assembly as drivers of sediment-hosted Pb–Zn mineralization in the Mount Isa region, northern Australia. J. Geol. Soc. Lond. 174, 773–786.

Giles, D., Betts, P., Lister, G., 2002. Far-field continental backarc setting for the 1.80–1.67 Ga basins of northeastern Australia. Geology 30, 823–826.

Glencore, 2019. Resources and Reserves Report: December 31, 2019, p. 71. http s://www.glencore.com/dam/jcr:0e7b6c0f-e670-49fe-9048-8582e7530dab/GL EN_2019_Resources_Reserves_Report–.pdf.

Grant, J.A., 1986. The isocon diagram; a simple solution to Gresens' equation for metasomatic alteration. Econ. Geol. 81, 1976–1982.

Grant, J.A., 2005. Isocon analysis: a brief review of the method and applications. Phys. Chem. Earth Parts A/B/C 30, 997–1004.

Hannan, K.W., Golding, S.D., Herbert, H.K., Krouse, H.R., 1993. Contrasting alteration assemblages in metabasites from Mount Isa, Queensland; implications for copper ore genesis. Econ. Geol. 88, 1135–1175.

Heinrich, C.A., Andrew, A.S., Wilkins, R.W.T., Patterson, D.J., 1989. A fluid inclusion and stable isotope study of synmetamorphic copper ore formation at Mount Isa, Australia. Econ. Geol. 84, 529–550.

Héroux, Y., Chagnon, A., Bertrand, R., 1979. Compilation and correlation of major thermal maturation indicators. Am. Assoc. Pet. Geol. Bull. 63, 2128–2144.

Hornibrook, E.R.C., Longstaffe, F.J., 1996. Berthierine from the lower cretaceous Clearwater formation, Alberta, Canada. Clay Clay Miner. 44, 1–21.

Humphris, S.E., Alt, J.C., Teagle, D.A.H., Honnorez, J.J., 1998. Geochemical changes during hydrothermal alteration of basement in the stockwork beneath the active TAG hydrothermal mound. In: Proceedings-Ocean Drilling Program Scientific Results. National Science Foundation, pp. 255–276.

Jackson, M.J., Scott, D.L., Rawlings, D.J., 2000. Stratigraphic framework for the Leichhardt and Calvert Superbasins: review and correlations of the pre-1700 Ma successions between Mt Isa and McArthur River. Aust. J. Earth Sci. 47, 381–403.

Johnson, B.R., Tostevin, R., Gopon, P., Wells, J., Robinson, S.A., Tosca, N.J., 2020. Phosphorus burial in ferruginous SiO2-rich Mesoproterozoic sediments. Geology 48, 92–96.

Kah, L.C., 2000. Depositional δ18O signatures in Proterozoic dolostones: constraints on seawater chemistry and early diagenesis. SEPM Spec. Publ. 67, 345–360.

Kennedy, M., Droser, M., Mayer, L.M., Pevear, D., Mrofka, D., 2006. Late Precambrian oxygenation; inception of the clay mineral factory. Science 311, 1446–1449.

Kretz, R., 1982. A model for the distribution of trace elements between calcite and dolomite. Geochim. Cosmochim. Acta 46, 1979–1981.

Lambert, I.B., Scott, K.M., 1973. Implications of geochemical investigations of sedimentary rocks within and around the McArthur zinc-lead-silver deposit, Northern Territory. J. Geochem. Explor. 2, 307–330.

Lanson, B., Besson, G., 1992. Characterization of the end of smectite-to-illite transformation: Decomposition of X-ray patterns. Clay Clay Miner. 40, 40–52.

Lanson, B., Champion, D., 1991. The I/S-to-illite reaction in the late stage diagenesis. Am. J. Sci. 291, 473–506.

Large, R.R., McGoldrick, P.J., 1998. Lithogeochemical halos and geochemical vectors to stratiform sediment hosted Zn–Pb–Ag deposits, 1. Lady Loretta Deposit, Queensland. J. Geochem. Explor. 63, 37–56.

Large, R.R., Bull, S.W., Cooke, D.R., McGoldrick, P.J., 1998. A genetic model for the HYC Deposit, Australia; based on regional sedimentology, geochemistry, and sulfide-sediment relationships. Econ. Geol. 93, 1345–1368.

Large, R.R., Bull, S.W., McGoldrick, P.J., 2000. Lithogeochemical halos and geochemical vectors to stratiform sediment hosted Zn–Pb–Ag deposits: part 2. HYC deposit, McArthur River, Northern Territory. J. Geochem. Explor. 68, 105–126.

Large, R.R., Bull, S.W., McGoldrick, P.J., Walters, S.G., 2005. Stratiform and strata-bound Zn-Pb-Ag deposits in Proterozoic sedimentary basins, northern Australia. Econ. Geol. 100, 931–963.

Leach, D.L., Sangster, D.F., Kelley, K.D., Large, R.R., Garven, G., Allen, C.R., Gutzmer, J., Walters, S., 2005. Sediment-hosted lead-zinc deposits: a global perspective. Econ. Geol. 100, 561–607.

Leach, D.L., Bradley, D.C., Huston, D., Pisarevsky, S.A., Taylor, R.D., Gardoll, S.J., 2010. Sediment-hosted lead-zinc deposits in Earth history. Econ. Geol. 105, 593–625.

Lynch, F.L., Mack, L.E., Land, L.S., 1997. Burial diagenesis of illite/smectite in shales and the origins of authigenic quartz and secondary porosity in sandstones. Geochim. Cosmochim. Acta 61, 1995–2006.

Magnall, J.M., Gleeson, S.A., Hayward, N., Rocholl, A., 2020. Massive sulfide Zn deposits in the Proterozoic did not require euxinia. Geochem. Perspect. Lett. 13, 19–24. https://doi.org/10.7185/geochemlet.2008.

Mathias, B.V., Clark, G.J., 1975. Mount Isa copper and silver-lead-zinc orebodies—Isa and Hilton mines. Econ. Geol. Aust. Papua New Guinea Aust. Inst. Min. Metall. 1, 351–372.

McClay, K.R., 1979. Folding in silver-lead-zinc orebodies, Mount Isa. Australia. Trans. Inst. Min. Metall. Sect. B Appl. Earth Sci. 88, B5–B14.

McGoldrick, P., Winefield, P., Bull, S., Selley, D., Scott, R., 2010. Sequences, synsedimentary structures, and sub-basins: the where and when of SEDEX zinc systems in the southern McArthur Basin, Australia. Soc. Econ. Geol. Spec. Publ. 15, 1–23.

Mering, J.A., Barker, S.L.L., Huntington, K.W., Simmons, S., Dipple, G., Andrew, B., Schauer, A., 2018. Taking the temperature of hydrothermal ore deposits using clumped isotope thermometry. Econ. Geol. 113, 1671–1678.

Merriman, R.J., Frey, M., 1999. Patterns of very low-grade metamorphism in metapelitic rocks. In: Frey, M., Robinson, D. (Eds.), Low-Grade Metamorphism, pp. 61–107.

Moore, D.M., Reynolds Jr., R.C., 1997. X-Ray Diffraction and the Identification and Analysis of Clay Minerals (2nd Ed.): Oxford University Press. Oxford University Press, Oxford, England, p. 378.

Morad, S., Al-Ramadan, K., Ketzer, J.M., De Ros, L.F., 2010. The impact of diagenesis on the heterogeneity of sandstone reservoirs: a review of the role of depositional facies and sequence stratigraphy. Am. Assoc. Pet. Geol. Bull. 94, 1267–1309.

Murphy, T.E., 2004. Structural and Stratigraphic Controls on Mineralization at the George Fisher Zn-Pb-Ag Deposit, Northwest Queensland, Australia. Unpubl. PhD Thesis. James Cook University, p. 403.

Nance, W.B., Taylor, S.R., 1976. Rare earth element patterns and crustal evolution—I. Australian post-Archean sedimentary rocks. Geochim. Cosmochim. Acta 40, 1539–1551.

Nesbitt, Hw, Young, G.M., 1982. Early Proterozoic climates and plate motions inferred from major element chemistry of lutites. Nature 299, 715–717.

Neudert, M., 1983. A Depositional Model for the Upper Mount Isa Group and Implications for Ore Formation. Unpubl. PhD Thesis. Australian National University, p. 538.

Odin, G.S., Matter, A., 1981. De glauconiarum origine. Sedimentology 28, 611–641.

Page, R.W., Bell, T.H., 1986. Isotopic and structural responses of granite to successive deformation and metamorphism. J. Geol. 94, 365–379.

Page, R.W., Sweet, I.P., 1998. Geochronology of basin phases in the western Mt Isa Inlier, and correlation with the McArthur Basin. Aust. J. Earth Sci. 45, 219–232.

Page, R.W., Jackson, M.J., Krassay, A.A., 2000. Constraining sequence stratigraphy in north Australian basins: SHRIMP U–Pb zircon geochronology between Mt Isa and McArthur River. Aust. J. Earth Sci. 47, 431–459.

Painter, M.G.M., 2003. The Geochemical and Mineralogical Haloes Around the Mt Isa Base Metal Orebodies. Unpubl. PhD Thesis. University of Queensland, p. 478.

Painter, M.G.M., Golding, S.D., Hannan, K.W., Neudert, M.K., 1999. Sedimentologic, petrographic, and sulfur isotope constraints on fine-grained pyrite formation at Mount Isa Mine and environs, Northwest Queensland, Australia. Econ. Geol. 94, 883–912.

Perkins, W.G., 1998. Timing of formation of Proterozoic stratiform fine-grained pyrite; post-diagenetic cleavage replacement at Mount Isa? Econ. Geol. 93, 1153–1164.

Perkins, W.G., Bell, T.H., 1998. Stratiform replacement lead-zinc deposits; a comparison between Mount Isa, Hilton, and McArthur River. Econ. Geol. 93, 1190–1212.

Rafiei, M., Kennedy, M., 2019. Weathering in a world without terrestrial life recorded in the Mesoproterozoic Velkerri Formation. Nat. Commun. 10, 1–9.

Revie, D., Normington, V.J., 2020. Shale resource data from the greater McArthur Basin. In: Northern Territory, Geological Survey, Digital Information Package DIP 014. Version January 2020.

Rieger, P., Magnall, J.M., Gleeson, S.A., Lilly, R., Rocholl, A., Kusebauch, C., 2020a. Sulfur isotope constraints on the conditions of pyrite formation in the paleoproterozoic urquhart shale formation and George Fisher Zn-Pb-Ag Deposit, Northern Australia. Econ. Geol. 115, 1003–1020.

Rieger, P., Magnall, J.M., Gleeson, S.A., Schleicher, A.M., Bonitz, M., Lilly, R., 2020b. The Mineralogical and Lithogeochemical Footprint of the George Fisher Zn-Pb-Ag Massive Sulphide Deposit in the Proterozoic Urquhart Shale Formation, Queensland, Australia. GFZ Data Serv. https://doi.org/10.5880/GFZ.3.1.2020.003.

Riegler, T., McClenaghan, S.H., 2017. Authigenic potassic silicates in the Rathdowney Trend, Southwest Ireland: new perspectives for ore genesis from petrography of gangue phases in Irish-type carbonate-hosted Zn-Pb deposits. Ore Geol. Rev. 88, 140–155.

Rimstidt, J.D., Chermak, J.A., Schreiber, M.E., 2017. Processes that control mineral and element abundances in shales. Earth-Sci. Rev. 171, 383–399.

Rubenach, M.J., 1992. Proterozoic low-pressure/high-temperature metamorphism and an anticlockwise P–T–t path for the Hazeldene area, Mount Isa Inlier, Queensland, Australia. J. Metamorph. Geol. 10, 333–346.

Scott, C., Lyons, T.W., 2012. Contrasting molybdenum cycling and isotopic properties in euxinic versus non-euxinic sediments and sedimentary rocks: refining the paleoproxies. Chem. Geol. 324, 19–27.

Slack, J.F., Kelley, K.D., Anderson, V.M., Clark, J.L., Ayuso, R.A., 2004. Multistage hydrothermal silicification and Fe-Tl-As-Sb-Ge-REE enrichment in the Red Dog Zn-Pb-Ag district, northern Alaska: geochemistry, origin, and exploration applications. Econ. Geol. 99, 1481–1508.

Smith, W.D., 1969. Penecontemporaneous faulting and its likely significance in relation to Mount Isa ore deposition. Spec. Publ. Geol. Soc. Aust. 2, 225–235.

Southgate, P.N., Scott, D.L., Sami, T.T., Domagala, J., Jackson, M.J., James, N.P., Kyser, T.K., 2000. Basin shape and sediment architecture in the Gun Supersequence: a strike-slip model for Pb–Zn–Ag ore genesis at Mt Isa. Aust. J. Earth Sci. 47, 509–531.

Southgate, P.N., Neumann, N.L., Gibson, G.M., 2013. Depositional systems in the Mt Isa Inlier from 1800 Ma to 1640 Ma: implications for Zn–Pb–Ag mineralisation. Aust. J. Earth Sci. 60, 157–173.

Spinks, S.C., Peare, M., Ryan, C., Moorhead, G., Sheldon, H., Kunzmann, M., Liu, W., Blaikie, T., Schaubs, P., Kirkham, R., 2019. Carbonate replacement and thallium enrichment: ultra-high-resolution trace element mapping, and the origin of Proterozoic sediment-hosted Zn-Pb deposits. In: Proc. 15th SGA Bienn. Meet. Vol. 2 Life with Ore Depos. Earth, 15th Bienn. Meet. Soc. Geol. Appl. to Miner. Depos (Glasgow, Scotl. 2019).

Tang, D., Shi, X., Jiang, G., Zhou, X., Shi, Q., 2017. Ferruginous seawater facilitates the transformation of glauconite to chamosite: an example from the Mesoproterozoic Xiamaling Formation of North China. Am. Mineral. 102, 2317–2332.

Taylor, S.R., McLennan, S.M., 1995. The geochemical evolution of the continental crust. Rev. Geophys. 33, 241–265.

Valenta, R., 1994. Deformation of host rocks and stratiform mineralization in the Hilton Mine area. Mt Isa. Aust. J. Earth Sci. 41, 429–443.

Valenta, R.K., 1988. Deformation, fluid flow and mineralization in the Hilton area, Mt Isa, Australia. Unpub. PhD Thesis. Monash University, p. 284.

van den Heuvel, B.H., 1969. Sedimentation, stratigraphy and post-depositional changes in the sediments of the upper formations of the Mount Isa group, North-West Queensland. Unpubl. PhD Thesis. University of Queensland, p. 195.

Vine, J.D., Tourtelot, E.B., 1970. Geochemistry of black shale deposits; a summary report. Econ. Geol. 65, 253–272.

Virolle, M., Brigaud, B., Bourillot, R., Féniès, H., Portier, E., Duteil, T., Nouet, J., Patrier, P., Beaufort, D., 2019. Detrital clay grain coats in estuarine clastic deposits: origin and spatial distribution within a modern sedimentary system, the Gironde Estuary (south-West France). Sedimentology 66, 859–894.

Waring, C.L., 1990. Genesis of the Mount Isa copper ore system. Unpub. PhD Thesis. Monash University, p. 295.

Whitbread, M.A.I., 2004. Lithogeochemical Alteration Around the Century and Elura Zn-Pb-Ag Deposits: Detecting Alteration Expressions in the Deep and Near Surface Environments. Unpubl. PhD Thesis. University of Canberra, p. 410.

Wilkinson, J.J., Crowther, H.L., Coles, B.J., 2011. Chemical mass transfer during hydrothermal alteration of carbonates: Controls of seafloor subsidence, sedimentation and Zn–Pb mineralization in the Irish Carboniferous. Chem. Geol. 289, 55–75.

Wilson, C.J.L., 1972. The stratigraphic and metamorphic sequence west of Mount Isa, and associated igneous intrusions. Proc. Aust. Inst. Min. Metall. 243, 27–44.

Worden, R.H., Griffiths, J., Wooldridge, L.J., Utley, J.E.P., Lawan, A.Y., Muhammed, D. D., Simon, N., Armitage, P.J., 2020. Chlorite in sandstones. Earth-Sci. Rev. 204, 103105.

Wyborn, L.A.I., Page, R.W., McCulloch, M.T., 1988. Petrology, geochronology and isotope geochemistry of the post-1820 Ma granites of the Mount Isa Inlier: mechanisms for the generation of Proterozoic anorogenic granites. Precambrian Res. 40, 509–541.